

1 Targeting Oncogenic Src Homology 2 Domain-Containing Phosphatase 2 2 (SHP2) by Inhibiting its Protein-Protein Interactions 3

4 Running title: Inhibiting protein interactions of oncogenic SHP2 5

6 S. Bobone,¹ L. Pannone,^{2,3} B. Biondi,⁴ M. Solman,⁵ E. Flex,³ V. Canale,¹ P. Calligari,¹ C. De
7 Favari,⁶ T. Gandini,⁶ A. Quercioli,¹ G. Torini,¹ M. Venditti,² A. Lauri,² G. Fasano,^b J. Hoeksma,⁵
8 V. Santucci,¹ G. Cattani,¹ A. Bocedi,¹ G. Carpentieri,^{2,3} V. Tirelli,⁷ M. Sanchez,⁷ C. Peggion,⁶ F.
9 Formaggio,^{4,6} J. den Hertog,^{4,8} S. Martinelli,^{3,†} G. Bocchinfuso,^{1,†} M. Tartaglia,^{2,†} Lorenzo
10 Stella^{1,*}

11
12 1. Department of Chemical Sciences and Technologies, University of Rome Tor Vergata, Rome,
13 00133, Italy.

14 2. Genetics and Rare Diseases Research Division, Ospedale Pediatrico Bambino Gesù, IRCCS,
15 Rome, 00146, Italy.

16 3. Dipartimento di Oncologia e Medicina Molecolare, Istituto Superiore di Sanità, Rome, 00161,
17 Italy.

18 4. Institute of Biomolecular Chemistry, Padova Unit, CNR, Padova, 35131, Italy.

19 5. Hubrecht institute - KNAW and University Medical Center Utrecht, Utrecht, 3584 CT, The
20 Netherlands.

21 6. Department of Chemical Sciences, University of Padova, Padova, 35131, Italy.

22 7. Centre of Core Facilities, Istituto Superiore di Sanità, Rome, 00161, Italy.

23 8. Institute of Biology Leiden, Leiden University, Leiden, 2333 BE, the Netherlands.

24
25 † These authors contributed equally.

26
27 * To whom correspondence should be addressed:

28 Prof. Lorenzo Stella,

29 Department of Chemical Science and Technologies,

30 University of Rome Tor Vergata,

31 Via della Ricerca Scientifica, 1, 00133, Rome, Italy

32 Tel. +390672594463

33 stella@stc.uniroma2.it
34

35 **Abstract**

36 We developed a new class of inhibitors of protein-protein interactions of the SHP2 phosphatase,
37 which is pivotal in multiple signaling pathways and a central target in the therapy of cancer and
38 rare diseases. Currently available SHP2 inhibitors target the catalytic site or an allosteric pocket,
39 but lack specificity or are ineffective on disease-associated SHP2 mutants. Based on the
40 consideration that pathogenic lesions cause signaling hyperactivation due to increased SHP2
41 association with cognate proteins, we developed peptide-based molecules with low nM affinity
42 for the N-terminal Src homology domain of SHP2, good selectivity, stability to degradation and
43 an affinity for pathogenic variants of SHP2 up to 20 times higher than for the wild-type protein.
44 The best peptide reverted the effects of a pathogenic variant (D61G) in zebrafish embryos. Our
45 results provide a novel route for SHP2-targeted therapies and a tool to investigate the role of
46 protein-protein interactions in the function of SHP2.
47

48 Introduction

49 *SHP2 in physiology and pathology*

50 Tyrosine phosphorylation, regulated by protein-tyrosine kinases (PTKs) and protein-tyrosine phosphatases (PTPs), is
51 a fundamental mechanism of cell signaling. Aberrant tyrosine phosphorylation, caused by hyperactive PTKs, occurs
52 in many malignancies and most current targeted anticancer drugs are PTK inhibitors. PTPs counteract the effects of
53 kinases, and therefore they are generally considered negative regulators of cell signaling and tumor suppressors
54 [Elson 2018]. However, the Src homology 2 (SH2) domain-containing phosphatase 2 (SHP2), encoded by the
55 *PTPN11* gene, is a non-receptor PTP that does not conform to this simplistic picture [Tajan 2015].

56 SHP2 is ubiquitously expressed and mediates signal transduction downstream of various receptor tyrosine kinases
57 (RTKs): it is required for full and sustained activation of the RAS/MAP kinase pathway [Saxton 1997] and modulates
58 signaling also through the PI3K-AKT and JAK-STAT pathways, among others. Therefore, it is involved in the
59 regulation of multiple cell processes, including proliferation, survival, differentiation and migration [Tajan 2015].
60 Therefore, it is not surprising that dysregulated SHP2 function contributes to oncogenesis and underlies
61 developmental disorders [Tajan 2015].

62 *PTPN11* was the first proto-oncogene encoding a tyrosine phosphatase to be identified [Tartaglia 2003]. Somatic
63 acquired, gain of function mutations in *PTPN11* are the major cause of juvenile myelomonocytic leukemia (JMML),
64 accounting for approximately 35% of cases [Tartaglia 2003]. JMML is a rare and aggressive
65 myelodysplastic/myeloproliferative disorder of early childhood with a very poor prognosis, for which no drugs are
66 presently available. Somatic *PTPN11* mutations also occur in childhood myelodysplastic syndromes, acute monocytic
67 leukemia (AMoL, FAB M5) and acute lymphoblastic leukemia (ALL, “common” subtype) [Tartaglia 2003; 2004].
68 More rarely, activating mutations in this gene are found in adult myelodysplastic syndromes, chronic
69 myelomonocytic leukemia, as well as solid tumors, including neuroblastoma, glioma, embryonal rhabdomyosarcoma,
70 lung cancer, colon cancer and melanoma.

71 In addition to malignancies driven by *PTPN11* mutations, several forms of cancer are linked to the activity of wild
72 type (WT) SHP2, too. By screening hundreds of cancer cell lines with a shRNA library, a landmark study showed
73 that SHP2 is required for survival of receptor tyrosine kinases (RTK)-driven cancer cells [Chen 2016]. SHP2 is also a
74 central node in intrinsic and acquired resistance to targeted cancer drugs [Prahallad 2015], which is often caused by
75 RTK activation through feedback loops.

76 SHP2 is a mediator of immune checkpoint pathways, such as PD-1 [Okazaki 2013]. These signaling cascades inhibit
77 the activation of immune cells, thus allowing self-tolerance and modulation of the duration and amplitude of
78 physiological immune responses. SHP2 binds to the activated receptors and is responsible for starting the signaling
79 cascade that prevents immune cell activation [Okazaki 2013]. Some cancer cells are able to hijack these signaling
80 pathways, thus evading antitumor immune defenses; therefore, SHP2 is currently being considered as a possible
81 target for cancer immunotherapy [Marasco 2020]. Finally, it is worth mentioning that induction of gastric carcinoma
82 by *H. pylori* is mediated by the interaction of its virulence factor CagA with SHP2, causing aberrant activation of the
83 phosphatase [Higashi 2002, Hayashi 2017].

84 In addition to its role in cancer, SHP2 is involved in a family of rare diseases collectively known as RASopathies.
85 Germline missense mutations in *PTPN11* occur in ~50% of individuals affected by Noonan syndrome (NS)
86 [Tartaglia 2001], one of the most common non-chromosomal disorders affecting development and growth [Roberts
87 2013], and in ~90% of patients affected by the clinically related Noonan syndrome with multiple lentigines (NSML,
88 formerly known as LEOPARD syndrome) [Digilio 2002]. RASopathies are characterized by congenital cardiac
89 anomalies, hypertrophic cardiomyopathy, short stature, musculoskeletal anomalies, facial dysmorphisms, variable
90 intellectual disability and susceptibility to certain malignancies [Tartaglia 2010]. To date, the only treatment in use
91 for NS and related disorders is growth hormone therapy, to improve linear growth [Roberts 2013].

92 *Structure and allosteric regulation of SHP2*

93 The structure of SHP2 includes two Src homology 2 (SH2) domains, called N-SH2 and C-SH2, followed by the
94 catalytic PTP domain, and an unstructured C-terminal tail with a still uncharacterized function (Figure 1) [Tajan
95 2015]. SH2 domains are recognition elements that bind protein sequences containing a phosphorylated tyrosine (pY)
96 [Liu 2006, Anselmi 2020]. In SHP2, they mediate association to RTKs, cytokine receptors, cell adhesion molecules
97 and scaffolding adaptors. Therefore, SHP2 (together with the closely related SHP1) is recruited (through its SH2
98 domains) by motifs containing two pYs and dephosphorylates other (or even the same) pYs through its PTP domain.
99 The crystallographic structures of SHP2 [Hof 1998, LaRochelle 2018], complemented by biochemical analyses
100 [Keilhack 2005; Tartaglia 2006; Bocchinfuso 2007; Martinelli 2008], have elucidated the main features of the
101 allosteric regulation of SHP2 activity. Under basal conditions, the N-SH2 domain blocks the active site of the PTP
102 domain, inserting a loop (DE or “blocking” loop) in the catalytic pocket. Consistently, the basal activity of SHP2 is
103 very low. Association of SHP2 to its binding partners through the SH2 domains favors the release of this
104 autoinhibitory interaction, making the catalytic site available to substrates, and causing activation (Figure 1).
105 Specifically, structures of the N-SH2 domain associated to phosphopeptide sequences show that association to

106 binding partners induces a conformational change in the blocking loop, which loses complementarity to the active
107 site [Lee 1994]. At the same time, the N-SH2/PTP interaction allosterically controls the conformation of the N-SH2
108 domain binding site. Structures of the autoinhibited protein show that the binding site of the N-SH2 domain is closed
109 by two loops (EF and BG). By contrast, in structures of the isolated N-SH2 domain [Lee 1994], or the recently
110 reported structure of the active state of SHP2 [LaRochelle 2018], the binding site is open (Figure 1). Consequently,
111 we and others have hypothesized that the transition between the closed, autoinhibited state and the open, active
112 conformation is coupled to an increased affinity for binding partners [Keilhack 2005; Bocchinfuso 2007, Martinelli
113 2008, LaRochelle 2018].

114 The spectrum of pathogenic *PTPN11* mutations is generally consistent with this picture of SHP2 regulation. Most
115 mutations cluster at the N-SH2/PTP interface, destabilizing the interaction between these two domains and causing
116 constitutive activation of the phosphatase [Keilhack 2005; Tartaglia 2006; Bocchinfuso 2007]. These mutations
117 concomitantly induce an increased responsiveness to activation by association of bisphosphorylated sequences to the
118 SH2 domains [Keilhack 2005; Bocchinfuso 2007; Martinelli 2008; LaRochelle 2018]. Other mutations localize in the
119 binding site of the SH2 domains, and simply cause an increased affinity for phosphorylated binding partners
120 [Tartaglia 2006]. In all cases, the final effect is an upregulation of the RAS/MAPK signal transduction pathway.

121 *SHP2 as a pharmacological target*

122 All the findings reported above clearly indicate SHP2 as an important molecular target for cancer and RASopathies
123 [Tang 2020]. Since SHP2 is a convergent node for multiple signaling pathways, SHP2 inhibitors may represent a way
124 to suppress the effect of disease-causing mutations involving different proteins along the signaling cascade with a
125 single molecule [Mullard 2018].

126 Research efforts in SHP2-targeted drug discovery have been focused mainly on active-site inhibitors. Several
127 molecules inhibiting the catalytic activity of SHP2 have been reported, but many of them are affected by the same
128 limitations that led PTPs in general to be considered “undruggable”, *i.e.* lack of target specificity and poor
129 bioavailability [Mullard 2018]. Some compounds with good affinity and apparent selectivity have been described, but
130 more recent studies demonstrated that these molecules have several off-target effects [Tsutsumi 2018].

131 An alternative pharmacological strategy has been pursued by researchers at Novartis [Chen 2016], followed by others
132 [Mullard 2018; Tang 2020], who reported allosteric inhibitors stabilizing the autoinhibited structure of SHP2 by
133 binding to a pocket located at the interdomain interface in the closed conformation of the phosphatase. SHP099, the
134 inhibitor developed by Novartis, is finding promising applications in the treatment of RTK-driven cancers [LaMarche
135 2020] and in combined therapy against drug resistant cells [Prahallad 2015]. These results have spurred a renewed
136 interest in the inhibition of phosphatases [Mullard 2018]. Currently, several allosteric inhibitors stabilizing the closed
137 conformation of SHP2 are undergoing clinical trials [Tang 2020]: TNO155 by Novartis (derived from SHP099),
138 RMC-4630, by Revolution Medicines and Sanofi, JAB-3068 and JAB-3312, developed by Jacobio Pharmaceuticals
139 and RLY-1971, by Relay Therapeutics. However, these compounds are generally poorly effective in the case of
140 activating *PTPN11* mutants, since the allosteric binding site is lost in the open conformation of the enzyme
141 [LaRochelle 2018, Tang 2020].

142 *Inhibition of protein-protein interactions as an alternative pharmacological strategy*

143 Due to the allosteric mechanism described above, SHP2 activation and its association to binding partners are coupled
144 events. Therefore, the effect of NS- and leukemia-causing mutations destabilizing the autoinhibited conformation is
145 twofold: they cause an increase in the phosphatase activity of the protein, but at the same time favor the N-SH2
146 conformation suitable for binding phosphorylated proteins, thus increasing the overall responsiveness of SHP2 to its
147 interaction partners. Several lines of evidence indicate that the second event, rather than the enhanced basal activity,
148 is essential for the abnormal activation of the RAS/MAPK pathway.

149 Some pathogenic mutations, such as the NS-associated p.T42A, simply increase the binding affinity of the N-SH2
150 domain, without causing basal activation [Martinelli 2008, Keilhack 2005]; on the other hand, the ability of SHP2 to
151 associate to binding partners is preserved in all the disease-associated *PTPN11* mutations [Tartaglia 2006, Martinelli
152 2012, 2020].

153 Truncated constructs with deletion or partial deletion of the N-SH2 domain cause a dramatic increase in the
154 enzymatic activity of SHP2 and, at the same time, a complete loss of its ability to bind signaling partners. These
155 constructs do not affect development in heterozygous mice [Saxton 1997] and do not cause any aberrant phenotype in
156 cells [Saxton 1997, Higashi 2002]. Indeed, RAS/MAPK signaling in homozygous cells with the mutated construct
157 was reduced with respect to the WT cells [Shi 1998]. However, cellular morphological changes (hummingbird
158 phenotype) were observed when the truncated construct was targeted to cellular membranes by adding a membrane-
159 localization signal [Higashi 2002], demonstrating the importance of proper cellular localization, normally mediated
160 by SH2 domains. The relevance of SHP2 association to its binding partners for its role in aberrant signaling has been
161 demonstrated also by a study on monobodies targeting the N-SH2 domain and disrupting its association with adaptor
162 proteins. Expression of these monobodies in cancer cells carrying the activating *p.V45L* mutation abolished ERK1/2

163 phosphorylation almost completely [Sha 2013]. Similarly, Kertész and coworkers [Kertész 2006] reported that the
164 natural SHP2-binding motif of Gab1, when delivered into immune cells, modulated phosphorylation patterns.
165 An example of the opposite situation, where binding is preserved and the catalytic activity is impaired, is provided by
166 *PTPN11* mutations causing NSML, such as T468M. This class of amino acid substitutions are located in proximity of
167 the PTP active site, at the PTP/N-SH2 interface, and have a twofold effect: they destabilize the closed state of the
168 protein, and consequently promote SHP2 association to signaling partners; at the same time, they perturb the active
169 site and therefore strongly impair the catalytic activity of the phosphatase. Interestingly, the phenotype of NSML is
170 very similar to that of NS, and these mutations still allow the activation of multiple effector pathways [Martinelli
171 2008; Yu 2014].

172 Overall, these findings strongly suggest that a mere enhancement in SHP2 catalytic activity is not sufficient to cause
173 disease and indicate that increased association to binding partners plays a major role in the pathogenic mechanism
174 associated with *PTPN11* mutations. Therefore, inhibition of SHP2 binding to other proteins through its SH2 domains
175 represents a promising alternative pharmaceutical strategy. Although SH2 domains in general have received much
176 attention as potential targets of pharmaceuticals [Machida 2005], no molecules targeting the SH2 domains of SHP2
177 for therapeutic purposes have been developed so far.

178 Based on these considerations, we explored the possibility to target SHP2 protein-protein interactions (PPIs), rather
179 than its catalytic activity. We developed a peptide-based molecule with low nM affinity to the N-SH2 domain of
180 SHP2, high specificity and resistance to degradation. This inhibitor rescued the mortality and developmental defects
181 induced by a pathogenic mutation *in vivo*. Our results provide a novel route for SHP2-targeted therapies and offer a
182 new tool to further investigate the role of SHP2 PPIs in the signaling cascades controlled by this phosphatase.
183

184 Results

185 1) Characterization of IRS-1 pY1172/N-SH2 binding

186 1.1) The IRS-1 pY1172 peptide binds the N-SH2 domain with a low nanomolar affinity

187 We recently characterized the structural determinants of peptides with high affinity and selectivity for the N-SH2
188 domain of SHP2 [Anselmi 2020]. The peptide corresponding to pY 1172 (rat sequence, SLN-pY-IDLDLVKD) or pY
189 1179 (human sequence, GLN-pY-IDLDLVKD) of insulin receptor substrate 1 (IRS-1) has one of the highest known
190 binding affinities for this domain. Based on our study, the IRS-1 pY 1172 sequence is near to optimal under several
191 respects, since it has apolar residues at positions +1, +3 and +5, which point towards the hydrophobic groove in the
192 N-SH2 structure, and anionic amino acids at positions +2 and +4, which can interact with a peculiar KxK motif in the
193 BG loop [Anselmi 2020].

194 The binding affinity of the IRS-1 pY1172 peptide has been characterized in several literature studies. Unfortunately,
195 these results are extremely contradictory, as reported in Table S1, with dissociation constants ranging from ~10 nM to
196 ~10 μ M. Several possible factors can be invoked to explain these discrepancies, including the effect of radioactive
197 labels [Case 1994], dimerization of GST-N-SH2 constructs [Sugimoto 1994, Ladbury 1995] even at low nM
198 concentrations [Fabriani 2009], or the sensitivity of the technique [KeliHack 2005]

199 Considering these difficulties, in the present study, we developed a fluorescence anisotropy binding assay. In a direct
200 binding experiment, the fluorescently labeled peptide IRS-1 pY1172 analog CF-P9 (Table 1) was titrated with
201 increasing concentrations of the N-SH2 domain. The fraction of protein-bound peptide was determined from the
202 increase in fluorescence anisotropy (Figure 2), and a K_d of 53 ± 2 nM was obtained (Table 2).

203 1.2) Phosphorylation contributes only 30% of the standard binding free energy

204 Association of SH2 domains with the partner proteins is regulated by phosphorylation, and therefore the phosphate
205 group is necessarily responsible for a large fraction of the binding affinity. On the other hand, to have a good
206 selectivity, the rest of the sequence must also contribute significantly to the peptide/protein interaction. To quantify
207 this aspect, we performed a binding experiment (Figure 2) with an unphosphorylated analog of the labeled IRS-1
208 pY1172 peptide, CF-P9Y0 (Table 1). The affinity was approximately 100 times lower, with a K_d of 6.6 ± 0.6 μ M,
209 compared with 53 ± 2 nM for the phosphorylated peptide. The corresponding values for the standard free energy of
210 binding (assuming a 1 M standard state) are -29.6 ± 0.2 kJ/mol and -41.6 ± 0.1 kJ/mol, respectively. Assuming
211 additivity of contributions, the phosphate group results to be responsible for the difference of -12.0 ± 0.2 kJ/mol, *i.e.*
212 for less than 30% of the total standard binding free energy of the phosphorylated peptide. This result indicates that the
213 contribution of the rest of the peptide predominates in the binding interactions and bodes well for our design efforts.

214 2) *Sequence optimization*

215 2.1) The sequence can be reduced to 8 amino acids without loss in affinity

216 Literature data are partially contradictory regarding the effect of shortening the IRS-1 pY1172 sequence on the
217 binding affinity. Kay [1998] reported that the sequence could be shortened at the C-terminus down to the +5 residue
218 and at the N-terminus down to the -2 position, without any loss in affinity. By contrast, Case [1994] observed a
219 significant reduction in affinity by shortening the sequence from SLN-pY-IDLDLVKD to LN-pY-IDLDLV. Our
220 previous study clearly indicated that residues -2 to +5 are the most important for the interaction [Anselmi 2020]. To
221 clarify the role of N-terminal residues in determining the N-SH2 domain binding affinity, we performed displacement
222 studies (Figure S1) with the unlabeled peptide P9, and with the shortened analogues P8 and P7 (Table 1), where
223 residues -3 or -2 and -3 were removed, respectively. No significant loss in affinity was observed by reducing the
224 sequence to 8 residues, while removal of the amino acid at position -2 caused a drastic perturbation of complex
225 stability (Figure S1). The -2 to +5 IRS-1 sequence is the minimal peptide with a low nM dissociation constant.
226

227 2.2) Single amino acids substitutions improve the K_d to the low nM range.

228 Hydrophobic residues are required at position +1, +3 and +5 of the phosphopeptide sequence [Anselmi 2020], but
229 aromatic residues are present in some natural high affinity binding sequences, at position +5 only [Case 1994, Hoyer
230 1995; Hayashi 2017, Bonetti 2018]. The crystallographic structures of some of these complexes [Lee 1994; Hayashi
231 2017] show that an aromatic side chain can be accommodated by a relatively large hydrophobic pocket and that the
232 +5 peptide residue interacts with the BG and EF loops of the domain, which are important for binding specificity
233 [Lee 1994, Anselmi 2020]. Finally, a preference for aromatic residues at position +5 has been indicated by several
234 peptide library studies [De Souza 2002; Imhof 2006; Martinelli 2012; Tinti 2013].

235 Based on these considerations, we analyzed in silico the effect of different aromatic amino acids at position +5. Free
236 energy calculations indicated that substitution of L with the bulkier W (but not with F) could be favorable (Figure 3).
237 The additional substitution of D in +4 with the longer E was evaluated as well, in view of a possible strengthening of
238 the electrostatic interactions with the KxK motif in the BG loop. However, in this case no further increase in binding
239 affinity was predicted by the free energy calculations (Figure 3).

240 Analogs with F or W at position +5 (P8F5 and P8W5), as well as a labeled analog with the L to W substitution (CF-
241 P9W5, Table 1) were synthesized and studied experimentally (Figure 4). As predicted, introduction of W in +5 was
242 highly favorable, leading to reduction in the dissociation constant by an order of magnitude, both for the labeled and
243 unlabeled analog (Tables 2 and 3). Consequently, the K_i for the P8W5 analog was 1.6 ± 0.4 nM. By contrast, the
244 additional D to E substitution resulted in a slight loss in binding affinity (Figure 4 and Table 2 and 3).
245 Based on these results, further studies concentrated on the peptide with W at position +5.

246 3) *Binding selectivity*

247 3.1) The modified sequence is highly selective for the N-SH2 domain of SHP2.

248 The selectivity of binding of CF-P9W5 was first assessed with respect to the C-SH2 domain of SHP2, again with the
249 fluorescence anisotropy assay (Figure S2). As reported in Table 2, the affinity for the C-SH2 domain was almost
250 1,000 times less than that for the N-SH2 domain.

251 A more complete analysis of the binding selectivity was performed on a protein array of 97 human SH2 domains
252 (Figure 5). An analogue of CF-P9W5 was employed in this assay, where CF was substituted with the Cy3 dye,
253 suitable for detection in the array reader. Control binding experiments showed that the change in fluorophore did
254 affect peptide binding affinity only marginally (Table 2). Strikingly, significant binding was observed only with the
255 N-SH2 domain of SHP2, and, to a lesser extent, to the SH2 domain of the adapter protein APS (also called SHP2B2).
256 It is worth noting that binding to the N-SH2 domain of SHP1, which has the highest identity with that of SHP2 [Liu
257 2006], was negligible.
258

259 4) *Engineering resistance to degradation*

260 4.1) Introduction of a non-hydrolysable pY mimic is compatible with low nM binding affinity

261 In view of intracellular or in vivo applications of the phosphopeptide, it is essential to make it resistant to
262 degradation. The most labile moiety is the phosphate group of the pY residue, which can be hydrolyzed by protein
263 tyrosine phosphatase, possibly also including SHP2, of which IRS-1 pY 1172 has been shown to be a substrate
264 [Noguchi 1994]. We substituted the pY with the non-hydrolysable mimetic phosphonodifluoromethyl phenylalanine
265 (F₂Pmp), which is isosteric with pY and has a total negative charge comparable to that of pY under physiologic pH
266 conditions [Burke 2006].

267 Binding experiments demonstrated that the substituted analogue (CF-P9ND0W5, where ND0 indicates the
268 introduction of the non-dephosphorylatable pY mimic at position 0, Table 1) has a dissociation constant for the N-
269 SH2 domain that is just an order of magnitude worse with respect to that of CF-P9W5 (68 ± 5 nM with respect to 4.6
270 ± 0.4 nM) (Figure S3 and Table 2). Similarly, the dissociation constant for the unlabeled peptide P9ND0W5 was $15 \pm$
271 0.4 nM (with respect to 1.6 ± 0.4 nM for P8W5) and thus remained in the nM range (Table 3).
272 For the sake of brevity, in the following text, CF-P9ND0W5 and its unlabeled analogue P9ND0W5 will be also
273 referred to as the optimized peptides, or CF-OP and OP, respectively.
274

275 4.2) The optimized peptide OP is resistant to proteolytic degradation

276 To test the resistance to proteases, the optimized peptide OP was incubated in human serum for up to 90 minutes, or
277 in DMEM for three days, and then analyzed by HPLC. No significant degradation was observed in these time frames
278 (Figure S4). By contrast, the octadecapeptide HPA3NT3 [Park 2008], which we used as a positive control, was
279 completely degraded already after 5 minutes (data not shown). This result bodes well for potential in vivo
280 applications of the peptide.
281

282 *5) Binding to and activation of the SHP2 protein*

283 5.1) OP binds to pathogenic mutants with much higher affinity than to the WT protein

284 As discussed in the introduction, we and others have hypothesized that, in its autoinhibited state, the conformation of
285 the N-SH2 domain prevents efficient association to binding partners, while SHP2 binding affinity to phosphorylated
286 sequences is maximized in the open, active state [Keilhack 2005; Bocchinfuso 2007, Martinelli 2008, LaRoche
287 2018]. This model has many relevant consequences, because it implies that pathogenic mutants have a twofold effect:
288 they increase the activity of the phosphatase, but also its affinity towards binding partners. In principle, both effects
289 could be the origin of the hyperactivation of the signal transduction pathways involved in the pathologies caused by
290 *PTPN11* mutations.

291 Notwithstanding the relevance of this aspect, to the best of our knowledge, no direct phosphopeptide binding
292 experiments to the whole SHP2 protein have ever been performed, possibly due to the fact that pY can be
293 dephosphorylated by the PTP domain. Now, OP and its fluorescent analogue CF-OP allow us to directly assess the
294 hypothesis described above. Figure 6 and Table 2 report the results of binding experiments performed with CF-OP
295 and WT SHP2 or the pathogenic mutants A72S, E76K, D61H, F71L and E76V. E76K is among the most common
296 somatic lesions associated with leukemia, and has never been observed as germline event in individuals with NS
297 [Tartaglia 2003, 2006], as it results in early embryonic lethality [Xu 2011]. This mutation is strongly activating, with
298 a basal activity of the corresponding mutant being at least 10 times higher than that of the WT protein. Conversely,
299 A72S is a germline mutation specifically recurring among subjects with NS. In this case, basal activation is only
300 twofold [Bocchinfuso 2007]. The D61H, F71L and E76V amino acid substitutions have been identified as somatic
301 events in JMML and other leukemias [Tartaglia 2003] and, when transmitted in the germline, they are associated with
302 a high prenatal lethality (M. Zenker, personal communication). Interestingly, we observed that the affinity for CF-OP
303 nicely parallels the basal activity of these mutants (Figure 6). This finding provides a first direct confirmation that the
304 closed, autoinhibited state has a lower affinity for the binding partners, compared to the open, active conformation.

305 5.2) OP is also an inhibitor of the PTP domain.

306 Based on previous reports of the dephosphorylation of IRS-1 pY 1172 by SHP2 [Noguchi 1994], we verified if P8
307 and P8W5 are also a substrate of this protein. These experiments were performed with a truncated SHP2 construct
308 lacking the N-SH2 domain (SHP2 $_{\Delta 104}$), as it is fully activated and was shown to be more stable and less prone to
309 aggregation compared to the isolated PTP domain [Martinelli 2020]. As reported in Figure S5, dephosphorylation
310 was indeed observed, although to a lower extent than for other phosphopeptides.
311

312 Using the non-dephosphorylatable peptide CF-OP, we measured directly binding to the PTP domain of SHP2 (Figure
313 S6 and Table 2). Significant association was observed, although with a much lower affinity than with the N-SH2
314 domain ($K_d = 10.0 \pm 0.8$ μ M). This finding indicates that in principle, the non-dephosphorylatable OP could act as a
315 double hit SHP2 inhibitor, acting on both PPIs and catalytic activity.
316

317 *6) OP effectively reverses the effects of D61G mutation in vivo.*

318 We used the zebrafish model system to explore the in vivo effect of the peptide. Zebrafish Shp2a is highly
319 homologous to human SHP2 (91.2% protein sequence identity); in particular, the sequence of the N-SH2 domain and
320 of the N-SH2/PTP interface are identical in the human and fish proteins. RASopathies-associated mutants, including

321 activating mutants of Shp2a, greatly impact zebrafish development. In humans, the D61G substitution has been found
322 in both NS and leukemia [Kratz 2005] and in animal models it induces both NS-like features and myeloproliferative
323 disease [Araki 2004]. Microinjection of synthetic mRNA encoding NS-associated mutants of Shp2 at the one-cell
324 stage induces NS-like traits [Jopling 2007]. During gastrulation, convergence and extension movement are affected,
325 resulting in oval-shaped embryos, with increased major/minor axis length ratio at 11 hpf [Jopling 2007]. Here we co-
326 injected Shp2a-D61G mRNA with OP in zebrafish embryos, to investigate whether OP rescues the defective cell
327 movements during gastrulation.

328 As shown in Figure 7 and Figure S7, we observed a dose-dependent decrease in Shp2a-D61G-induced major/minor
329 axis ratios, with a rescue of the phenotype that was significant at 5 μ M peptide concentration. On the other hand,
330 embryos injected with Shp2a-WT were almost perfect spheres at 11 hpf, and co-injection with 3 μ M peptide had no
331 impact on their shape. As expected, a large portion of Shp2a-D61G injected embryos were severely affected and they
332 died during embryonic development, whereas injection of WT Shp2a did not induce significant lethality. We
333 followed the survival of Shp2a-D61G injected embryos and observed a significant and dose dependent improvement
334 in the survival of embryos upon co-injection with 0.3 μ M, 3 μ M and 5 μ M OP (Figure 8). By contrast, lethality of
335 WT Shp2a embryos was not affected by co-injection of 3 μ M OP. Altogether, these results indicate that co-injection
336 of the OP rescued the developmental defects induced by a pathogenic, basally activated Shp2a variant, while it had
337 no effect on WT embryos.

338 Discussion

339 Our findings provide several insights in the interaction of phosphopeptides with SH2 domains, and in particular, with
340 the N-SH2 domain of SHP2.

341 Soon after their discovery, the affinities of SH2 domains for their binding partners (*i.e.* the dissociation constants)
342 were considered to fall in the 10-100 nM range [Pawson 1995]. However, it turned out that most of the binding
343 studies performed in that period were affected by experimental artifacts, leading to an overestimation of the binding
344 affinities [Ladbury 1995, Kuriyan 1997]. A reassessment of the affinity values led to a commonly accepted range in
345 the order of 0.1 to 10 μ M [Kuriyan 1997, Machida 2005, Wagner 2013]. Such moderate affinities are considered to
346 be crucial for allowing transient association and dissociation events in cell signaling. Consistently, SH2 domains
347 artificially engineered to reach low nanomolar affinities for phosphorylated sequences (known as superbinders)
348 [Kaneko 2012], by increasing the domain affinity for the pY residue, have detrimental consequences for signal
349 transduction.

350 In the case of the N-SH2 domain of SHP2, literature results on the affinity for the IRS-1 pY 1172 peptide were
351 contradictory, with dissociation constants varying by three orders of magnitude [Case 1994, Sugimoto 1994,
352 Keilhack 2005]. Here, we showed that, at least for this peptide, the dissociation constant is in the low nM range. For
353 the N-SH2 domain, similar affinities have been reported also for the GRB2-associated-binding protein 1 (Gab1), pY
354 627 [Koncz 2001], and Gab2, pY 614 [Bonetti 2018]; several other peptides have a dissociation constant within an
355 order of magnitude of that of IRS-1 pY 1172 [Anselmi 2020]. In addition, in the present study, we were able to
356 further improve the affinity with respect to the parent peptide. Therefore, the N-SH2 domain of SHP2 might
357 constitute an exception in the panorama of SH2 domains, regarding the binding affinity. In most cases, interaction of
358 phosphopeptides with SH2 domains is dominated by the hydrophobic effect (except for the pY pocket). The N-SH2
359 domain of SHP2 has a peculiar KxK motif in the region of the BG loop pointing towards the binding groove, which
360 can interact electrostatically with basic residues present in the peptide sequence at positions +2 and +4 [Anselmi
361 2020]. Therefore, by contrast to the superbinders, the high binding affinity of the N-SH2 domain is a result of
362 additional interactions in the selectivity-determining region, and not in the pY pocket. Indeed, our data showed that
363 the pY phosphate contributed less than 30% of the standard binding free energy. This finding is comparable to what
364 has been reported for other SH2 domains [Waksman 2004].

365 Our data also showed that residue -2 contributes significantly to the binding affinity. Indeed, while the specificity of
366 most SH2 domains is determined by residues C-terminal to the pY, peptide library and array studies have shown that,
367 contrary to most other SH2 domains, the N-SH2 domain of SHP2 has specific preferences for position -2 [Anselmi
368 2020]. This peculiarity is due to the fact that, in place of the commonly conserved arginine at position 2 in the first α -
369 helix (α A2), the N-SH2 domain of SHP2 has G13. As a consequence, a hydrophobic peptide residue at position -2
370 can insert in the space left free by the missing protein side chain and interact with V14 α A3 and with the phenol ring
371 of pY, stabilizing its orientation and the overall complex [Anselmi 2020].

372 A preference of the N-SH2 domain of SHP2 for hydrophobic residues at positions +1, +3 and +5 is well established.
373 These side chains insert in the groove on the surface of the domain and interact with exposed hydrophobic patches
374 [Anselmi 2020]. Now our data demonstrate that the bulky, aromatic side chain of tryptophan at position +5 is 10
375 times better (in terms of dissociation constant) than the leucine residue, which is present in high-affinity natural
376 sequences such as those of IRS-1, Gab1 and Gab2. Overall, these data confirm that the phosphopeptide sequence in
377 the -2 to +5 stretch contributes significantly to the binding affinity. In principle, highly specific binding should be
378 possible.

379 In general, SH2 domains are only moderately discriminating for binding target sequences, and a range of residues is
380 tolerated at each site [Kuriyan 1997, Waksman 2004]. Consequently, nonspecific tyrosine phosphorylated sequences
381 are usually bound only 10- to 100-fold more weakly than specific targets [Bradshaw 1998, Waksman 2004, Machida
382 2005, Wagner 2013]. Indeed, additional specificity is often provided by tandem SH2 domains [Waksman 2004]: two
383 closely-spaced tyrosine phosphorylated motifs bind to tandem SH2 domains with 20- to 50-fold greater affinity and
384 specificity compared with the binding of a single SH2 domain with a single tyrosine phosphorylated motif [Wagner
385 2013]. SHP2 and its SH2 domains are no exception in this case, as peptide library and array studies, together with the
386 sequences of known natural binding partners, showed a significant variability in the sequences of peptides bound by
387 SHP2 [Anselmi 2020]. However, our results indicate that some peptides (like those developed here) can bind
388 specifically to a single SH2 domain. Among an array of 97 human SH2 domains, we found some interference only
389 with adapter protein APS (also called SHP2B2). The structure of the APS SH2 domain in complex with a cognate
390 protein shows that the phosphorylated sequence binds in a folded, kinked conformation, rather than in the usual
391 extended binding mode [Hu 2003]. This observation should facilitate the further development of our peptides, to
392 avoid the unwanted interaction with APS, without affecting the affinity for the target N-SH2.
393 Finally, it is worth mentioning that approximately one order of magnitude in affinity was lost by substituting the pY
394 residue with the non-dephosphorylatable mimic F₂Pmp. This finding is consistent with previous studies showing that
395 F₂Pmp is tolerated differently by various SH2 domains, and its insertion in place of pY in a phosphopeptide sequence
396 can lead either to a loss or to an increase in affinity, by approximately one order of magnitude [Burke 2006]. Further
397 optimization of this aspect is warranted, but the dissociation constant of our non-dephosphorylatable peptide
398 remained in the nM range.
399 The non-dephosphorylatable peptide allowed novel experiments on several aspects of SHP2 function and regulation.
400 As discussed in the introduction, in the autoinhibited state of SHP2, the N-SH2 binding groove is closed, apparently
401 making phosphopeptide association impossible. By contrast, the N-SH2 binding site is open in the structure of the
402 isolated N-SH2 domain or of active SHP2. Consequently, it has been hypothesized that mutations destabilizing the
403 closed state and favoring SHP2 activation could lead to an increase binding affinity [Bocchinfuso 2007]. This idea is
404 indirectly supported by the fact that basally activated mutants require lower concentrations of SH2 domain-binding
405 phosphopeptides to reach full activation [Keilhack 2005; Bocchinfuso 2007, Martinelli 2008, LaRochelle 2018].
406 However, no direct measurements of phosphopeptide binding to different SHP2 variants had been reported until now.
407 Our data directly demonstrate that the affinity for phosphopeptides of activated variants of SHP2 can increase by a
408 factor of 20, reaching the same value as the isolated domain in the most active mutants (Figure 6). This consequence
409 of pathogenic mutations adds to the increase in basal activity and might be the main responsible for hyperactivation
410 of signaling pathways modulated by SHP2. Interestingly, in view of possible therapeutic applications, in a cellular
411 environment, our peptide would act as an effective inhibitor of the PPIs of mutant, hyperactivated SHP2, while it
412 would have a much lower effect on the WT protein. This behavior is the exact opposite of what has been observed for
413 allosteric inhibitors, such as SHP099, which have a significantly impaired activity in pathogenic variants of SHP2
414 [LaRochelle 2018; Tang 2020].
415 A second link between SHP2 activity and binding functions is provided by literature data indicating for SHP2
416 interactors a role both as ligands of the SH2 domains and as substrates of the catalytic PTP domain, often with the
417 same phosphorylated sequence. Examples include IRS-1 [Sugimoto 1994, Noguchi 1994], Gab1 [Cunnick 2001,
418 Zhang 2002], Gab2 [Gu 1997], PDGFR [Rönnstrand 1999, Sugimoto 1992], PD-1 [Marasco 2020] and SHPS-1
419 [Fujioka 1996, Takada 1998]. We also showed here that our modified sequence can be dephosphorylated. These data
420 indicate the possible presence of a still uncharacterized feedback mechanism to regulate SHP2 signaling. Using our
421 non-dephosphorylatable peptide, we could demonstrate that a N-SH2-binding sequence associates to the catalytic
422 PTP domain, too, although with a lower affinity. This finding suggests that it might be possible to develop double-
423 edged sword molecules, able to inhibit both the catalytic activity and the PPIs of SHP2.
424 Inhibition of PPIs, particularly using peptides, is currently a hot area of pharmaceutical research. For the RAS/MAPK
425 pathway alone, at least 30 inhibitors of PPI have been developed and several of them are undergoing clinical trials
426 [García-Gómez 2018]. However, no studies on SHP2 have been reported, notwithstanding the central role of this
427 phosphatase in the pathway. Peptides are particularly appealing for the inhibition of PPIs, where large interfaces are
428 involved, which are difficultly targeted selectively by small molecules. An increasing number of drugs based on
429 peptides or peptidomimetics is progressing in the drug development pipeline [Henninot 2018]. Possible challenges in
430 the therapeutic applications of peptide-based molecules are their rapid degradation and a poor cell uptake, particularly
431 for highly charged sequences [Henninot 2018]. Here we successfully overcame the first hurdle, thanks to the
432 introduction of non-natural amino acids. Several studies have demonstrated that efficient intracellular delivery of
433 phosphopeptide mimics is possible, for instance by conjugation to cell-penetrating sequences [Nasrolahi Shirazi
434 2013]. Optimization of the cell uptake of our molecules, through different strategies, is currently underway.
435 Our *in vivo* findings on zebrafish embryos are very promising in view of potential applications, particularly
436 considering that the peptide is more effective on activating mutants than on the WT protein, contrary to allosteric
437 inhibitors such as SHP099 [LaRochelle 2018, Tang 2020]. Indeed, besides their possible use as a research tool to
438 study the role of PPIs in the function of SHP2, and regulation of the pathways controlled by this protein, including
439 RAS/MAPK and PI3K/AKT signaling, the reported peptides constitute lead compounds for the development of new

440 drugs against malignancies driven by *PTPN11* mutations, such as JMML, AMoL, and ALL, also considering that
441 allosteric inhibitors have low activity against basally activated SHP2 variants [Larochelle 2018, Tang 2020]. Finally,
442 another possible field of therapeutic application is represented by rare diseases such as NS and NSML, which are
443 caused by activating mutations of *PTPN11* (against which the available allosteric inhibitors are poorly active) and
444 cause several severe postnatal, evolutive clinical manifestations, particularly hypertrophic cardiomyopathy [Tartaglia
445 2010].
446

447 **Materials and methods**

448 *Materials*

449 Fmoc (9-fluorenylmethyloxycarbonyl)-amino acids were obtained from Novabiochem (Merck Biosciences, La Jolla,
450 CA). Rink amide MBHA resin (0.65 mmol/g, 100-200 mesh) was purchased from Novabiochem. All other protected
451 amino acids, reagents and solvents for peptide synthesis were supplied by Sigma–Aldrich (St. Louis, MO). The LB
452 medium components, all the reagents used to prepare the buffers and the Bradford reagent were purchased from
453 Sigma Aldrich. Tris(2-carboxyethyl)phosphine (TCEP) was obtained from Soltec Ventures, Beverly, MA, USA.
454 Spectroscopic grade organic solvents were purchased from Carlo Erba Reagenti (Milano, Italy). Cell culture media
455 growth factors and antibodies were purchased from VWR International PBI (Milan, Italy), EuroClone (Milan, Italy),
456 Promega (Madison, WI, USA), Invitrogen (Carlsbad, CA, USA), Cell Signaling (Danvers, MA, USA), Sigma-
457 Aldrich (Saint Louis, MO, USA), and Santa Cruz Biotechnology (Dallas, TX, USA).

458 *Peptide synthesis*

459 Assembly of peptides on the Syro Wave (Biotage, Uppsala, Sweden) peptide synthesizer was carried out on a 0.1
460 mmol scale by the FastMoc methodology, beginning with the Rink Amide MBHA resin (155 mg, loading 0.65
461 mmol/g). The peptide was cleaved from the resin, filtered and collected. The solution was concentrated under a flow
462 of nitrogen, and the crude peptide precipitated by addition on diethyl ether. The crude peptides were purified by
463 flash chromatography on Isolera Prime chromatographer (Biotage, Uppsala, Sweden) using a SNAP Cartridge KP-
464 C18-HS 12g or preparative RP-HPLC on a Phenomenex C18 column (22.1x250 mm, 10 μ m, 300 Å) using an Akta
465 Pure GE Healthcare (Little Chalfont, UK) LC system equipped with an UV-detector (flow rate 15 mL/min) and a
466 binary elution system: A, H₂O; B, CH₃CN/H₂O (9: 1 v/v); gradient 25-55% B in 30 min. The purified fractions were
467 characterized by analytical HPLC-MS on a Phenomenex Kinetex XB-C18 column (4.6 x 100 mm, 3.5 μ m, 100 Å)
468 with an Agilent Technologies (Santa Clara, CA) 1260 Infinity II HPLC system and a 6130 quadrupole LC/MS. The
469 binary elution system used was as follows: A, 0.05% TFA (trifluoroacetic acid) in H₂O; B, 0.05% TFA in CH₃CN;
470 flow rate 1 mL/min. Retention times (R_i) for the synthetic peptides obtained from RP-HPLC (the elution conditions
471 used for different peptides are listed in brackets) and molecular weights for the synthetic peptides experimentally
472 determined by ESI-MS spectrometry are reported in Table 1.

473 Peptides were dissolved in DMSO to obtain stock solutions between 1 and 1.5 mM. The exact concentration was
474 obtained by UV measurements, exploiting the signal of carboxyfluorescein for the labeled peptides and of pTyr, Tyr
475 and Trp for the unlabeled peptides. To this end, CF-labeled peptides were diluted from the stocks (1:100) in buffer
476 (pH 9), and their concentration was calculated from the CF signal at 490 nm using a molar extinction coefficient of
477 78000 M⁻¹ cm⁻¹ [Esbjörner 2007]. Unlabeled peptides were diluted 1:100 in a pH 7.4 buffer; molar extinction
478 coefficients of Tyr, Phe and Trp were taken from reference [Pace 1995], while molar extinction coefficient of pY
479 was taken from [Bradshaw 2003].

480 *Protein expression and purification*

481 The human esaHis-tagged *PTPN11* (residues 1-528) cDNA was cloned in a pET-26b vector (Novagen, MA, USA).
482 Nucleotide substitutions associated with NS or leukemia were introduced by site-directed mutagenesis (QuikChange
483 site-directed mutagenesis kit; Stratagene, CA, USA). A construct containing the cDNA encoding the isolated PTP
484 domain preceded by the C-SH2 domain (residues 105-528) was generated by PCR amplification of the full-length
485 wild-type cDNA and subcloned into the pET-26b vector (SHP2 Δ 104). A similar procedure was followed for the
486 constructs of the N-SH2 (residues 2-111), C-SH2 (109-217) and PTP (212-528) domains, and of the N-SH2/C-SH2
487 tandem (2-217). Primer sequences are available upon request.

488 Recombinant proteins were expressed as previously described [Martinelli 2012], using *E. coli* (DE3) Rosetta2
489 competent cells (Novagen). Briefly, following isopropyl β -D-1-thiogalactopyranoside (Roche) induction (2 hr at 30
490 °C, or overnight at 18 °C), bacteria were centrifuged at 5,000 rpm, 4 °C for 15 minutes, resuspended in a lysozyme-
491 containing lysis buffer (TRIS-HCl 50 mM, pH=8.5, NaCl 0.5 M, imidazole 20 mM, tris(2-carboxyethyl)phosphine
492 (TCEP) 1mM, lysozyme 100 mg/ml, 1 tablet of complete protease inhibition cocktail) and sonicated. The lysate was
493 centrifuged at 16,000 rpm, 4 °C for 30 minutes. The supernatant was collected and the protein of interest was purified
494 by affinity chromatography on a Ni-NTA column (Qiagen, Hilden, Germany), using a TRIS-HCl 50 mM, NaCl 0.5
495 M, TCEP 1 mM buffer containing 100 mM or 250 mM imidazole, for washing and elution, respectively. To remove

imidazole, the samples were then dialyzed in a 20 mM TRIS-HCl (pH 8.5) buffer, containing 1 mM TCEP and 1 mM EDTA and 50mM NaCl (or 150 mM NaCl if no further purification steps followed). Full length proteins and the SHP2 Δ 104 construct were then further purified by sequential chromatography, using an Äkta FPLC system (Äkta Purifier 900, Amersham Pharmacia Biotech, Little Chalfont, UK). The samples were first eluted within an anion exchange Hi-Trap QP 1ml-column (GE Helathcare, Pittsburgh, PA, USA); the elution was carried out using TRIS-HCl 20 mM (pH 8.5) in a NaCl gradient from 50 to 500 mM. The most concentrated fractions were then eluted in a gel filtration Superose column using TRIS-HCl 20 mM buffer containing NaCl (150 mM) as mobile phase. Sample purity was checked by SDS PAGE with Coomassie Blue staining and resulted to be always above 90%. Proteins were quantitated by both the Bradford assay and the UV absorbance of aromatic residues, calculating extinction coefficients according to [Pace 1995]. In general, the two methods were in agreement, but the values derived from UV absorbance were more precise and are reported in the Figures and Tables. The protein samples were used immediately after purification or stored at -20 °C and used within the following week. In this case, after thawing TCEP 2.5 mM was added, the samples were centrifuged at 13,000 rpm for 20 minutes, and the new concentration was re-evaluated. In the few cases where residual apparent absorbance due to light scattering was present in the UV spectra, it was subtracted according to [Castanho 1997].

511 *Phosphatase activity assays*

512 Catalytic activity was evaluated *in vitro* using 20 pmol of purified recombinant proteins in a 200 μ l reaction buffer
513 supplemented with 20 mM *p*-nitrophenyl phosphate (Sigma) as substrate, either basally or following stimulation with
514 the protein tyrosine phosphatase nonreceptor type substrate 1 (PTPNS1) bisphosphotyrosyl-containing motif (BTAM
515 peptide) (GGGGDIT(pY)ADLNLPKGKKPAPQAAEPNNHTE(pY)ASIQTS) (Primm, Milan, Italy), as previously
516 described [Martinelli 2008]. Proteins were incubated for 15 min (SHP2 Δ 104) or 30 min (SHP2) at 30 °C. Phosphate
517 release was determined by measuring absorbance at 405 nm.

518 DiFMUP (6,8-difluoro-4-methylumbelliferyl phosphate) assay was carried out as previously described [Chen 2016],
519 with minor changes. Briefly, reactions were performed at room temperature in 96-well flat bottom, low flange, non-
520 binding surface, black polystyrene plates (Corning, cat. no. 3991), using a final volume of 100 μ l and the following
521 assay buffer: 60 mM HEPES, pH 7.2, 75 mM NaCl, 75 mM KCl, 1 mM EDTA, 0.05% Tween-20, 5 mM DTT.

522 Catalytic activity was checked using 1 nM SHP2 and different concentrations of activating peptides. After 45 min at
523 25 °C, 200 μ M of surrogate substrate DiFMUP (Invitrogen, cat. no. D6567) was added to the mix, and incubated at
524 25 °C for 30 min. The reaction was stopped by addition of 20 μ l of 160 μ M bpV(Phen) (Potassium bisperoxo(1,10-
525 phenanthroline) oxovanadate (V) hydrate) (Enzo Life Sciences cat. no. SML0889-25MG). The fluorescence was
526 monitored using a microplate reader (Envision, Perkin-Elmer) using excitation and emission wavelengths of 340 nm
527 and 455 nm, respectively.

528 The ability of SHP2 to dephosphorylate the phosphopeptides was evaluated through a malachite green phosphatase
529 assay (PTP assay kit 1 Millipore, MA, USA). The BTAM peptide and the following monophosphorylated peptides
530 derived from known SHP2 substrates were used for comparison: DKQVEpYLDLDL (GAB1_{Y657}), EEENIp_YSVPHD
531 (p190A/RhoGAP_{Y1105}), and VDADEpYLIPQQ (EGFR_{Y1016}) (Primm). SHP2 Δ 104 (2.4 pmol) was incubated with 100
532 μ M of each phosphopeptide (total volume 25 μ l) for different times. The reaction was stopped by adding 100 μ l of
533 malachite green solution. After 15 min, absorbance was read at 655 nm, using a microplate reader, and compared
534 with a phosphate standard curve to determine the release of phosphate. Data obtained in the linear region of the curve
535 were normalized on the reaction time (1 min).

536 *Fluorescence anisotropy binding assay*

537 Anisotropy measurements were carried out using a Horiba Fluoromax 4 spectrofluorimeter.

538 For the binding assays, the requested peptide amount (1nM or 0.1 nM) was diluted in buffer (HEPES 10 mM, NaCl
539 150 mM, EDTA 1 mM, TCEP 1 mM, fluorescence buffer henceforth) and its anisotropy signal was recorded. The
540 peptide was then titrated with increasing protein amounts, until the anisotropy signal reached a plateau at its
541 maximum value, or up to a protein concentration where protein aggregation and consequent light scattering affected
542 the anisotropy values (usually above 1 μ M). The measurements of CF-labeled peptides were carried out using an
543 excitation wavelength of 470 nm and collecting the anisotropy values at an emission wavelength of 520 nm. A 495
544 nm emission filter was used. For the Cy3-labeled peptides, excitation and emission wavelengths of 520 and 560 nm
545 were used. The lowest peptide concentration needed to have a sufficient fluorescent signal (0.1 nM) was used in the
546 binding experiments. Higher concentrations (1 or 10 nM) were used for peptides with lower affinities, and therefore
547 higher K_d values.

548 The displacement assays were carried out with the same experimental settings. In this case, the labeled peptide-
549 protein complex was titrated with increasing amounts of the unlabeled peptide, following the decrease in anisotropy.
550 Measurements were carried out at the same CF-peptide concentration used for the corresponding binding
551 experiments. Regarding the protein concentration, a compromise between two requirements is needed [Huang 2003].
552 On one hand, it is desirable to have a significant fraction of the CF-peptide bound to the protein, to maximize the
553 dynamic range in the anisotropy signal, which decreases during the displacement experiment. On the other hand, the

554 protein concentration should be comparable or lower than the dissociation constant of the unlabeled peptide (K_i), to
555 allow a quantitative and reliable determination of its binding affinity. Since several unlabeled peptides had a higher
556 affinity than their fluorescent counterparts, in the displacement assays we used a protein concentration $[P]_T \sim K_d$, or in
557 some cases even $\sim K_d/2$.
558 The equations used for data fitting are described in the supplementary information appendix.

559 *SH2 domain microarray*

560 The microarray experiment was conducted by the Protein Array and Analysis Core at the MD Anderson Cancer
561 Center (University of Texas, USA), as previously described [Roth 2019]. Briefly, a library of SH2 domains [Huang
562 2008] was expressed as GST fusion in *E. coli* and purified on glutathione-sepharose beads. The domains were spotted
563 onto nitrocellulose-coated glass slides (Oncyte Avid slides, Grace Bio-Labs) using a pin arrayer. Each domain was
564 spotted in duplicate. After incubation with a Cy3-P9W5 solution (0.5, 5.0 nM, or 50 nM), fluorescence signals were
565 detected using a GeneTACTM LSIV scanner (Genomic Solutions).

566 *In silico studies*

567 System preparation

568 The initial structure of the N-SH2 complexed with phosphopeptide P8 (Table 1) was obtained by amino acid
569 substitutions (and deletions) in the crystallographic structure of the protein complexed with the GAB1 peptide
570 (sequence GDKQVE-pY-LDLDDL) (PDB code 4QSY). The obtained complex was then used as the starting
571 structure for subsequent amino acid substitutions in the bound peptide.

572 System equilibration

573 MD simulations were performed using the GROMACS 2018.2 simulation package [Abraham 2015] and a variant of
574 AMBER99SB force field with parameters for phosphorylated residues [Homeyer 2006]. Water molecules were
575 described by the TIP3P model. All the simulated systems were inserted in a pre-equilibrated triclinic periodic box
576 ($15 \times 7 \times 7 \text{ nm}^3$), containing about 24000 water molecules and counterions to neutralize system total charge. They were
577 relaxed first by doing a minimization with 5000 steepest descent cycles, by keeping protein positions fixed and
578 allowing water and ions to adjust freely, followed by a heating protocol in which temperature was progressively
579 increased from 100K to 300K. The system was then equilibrated for 100 ps in the NVT ensemble at 300 K, using
580 velocity rescaling with a stochastic term (relaxation time 1 ps) [Bussi 2007] and then for 500 ps at constant pressure
581 (1 atm) using the Parrinello-Rhman barostat (relaxation time 5 ps). Long-range electrostatic interactions were
582 calculated using the particle mesh Ewald method and the cut-off distance for the non-bonded interaction was set
583 equal to 12.0 Å. The LINCS constraint to all the hydrogen atoms and a 2 fs time-step were used.

584 Sampling of the initial configurations for Umbrella Sampling

585 For each system, a set of initial configurations was prepared by performing a center-of-mass (COM) pulling
586 simulation. The distance between the peptide and N-SH2 domain COMs was constrained with a harmonic force
587 ($K=1000 \text{ kJ mol}^{-1} \text{ nm}^{-2}$). Pulling was performed by gradually increasing the value of the equilibrium distance with a
588 constant-rate of 0.0025 nm/ps. The length of each simulation was about 2.5 ns. During the whole simulation, a
589 positional restraint ($1000 \text{ kJ mol}^{-1} \text{ nm}^{-2}$) was applied to all heavy atoms in the N-SH2 domain except for atoms in
590 loops around the binding region (residues 30-45, 52-75, 80-100). For the choice of the optimal unbinding pathway,
591 three different directions were tested, corresponding to: i) the vector from the phosphate to the alpha carbon in pY, in
592 the equilibrated complex; ii) the vector defined by the initial positions of the two COMs; iii) the vector perpendicular
593 to the surface of the cavity flanked by the EF and BG loops, passing through the N-SH2 domain center of mass.
594 Among the three different pathways, the third direction encountered less steric occlusion by the EF and BG loops,
595 and was thus selected for further analyses.

596 Umbrella sampling simulations

597 A set of starting configurations was extracted from the pull-dynamics trajectory saving the peptide-protein center-of-
598 mass distances every 2 Å in the range from 9 to about 40 Å, thus obtaining about 20 windows along the COM
599 distance. The system in each window was preliminarily equilibrated for 1ns with a strong positional restraint ($1000 \text{ kJ mol}^{-1} \text{ nm}^{-2}$)
600 to all carbon alpha atoms except for those in loops flanking the binding region (as in the pull simulation),
601 followed by a production run of 150 ns with the restraints. During this stage, a harmonic potential ($K=1000 \text{ kJ mol}^{-1} \text{ nm}^{-2}$)
602 was applied on the distance between the two COMs. Additional sampling windows were added every 1 Å along
603 the distance between the two COMs up to a distance of 15 Å. The resulting asymmetric distribution of sampling
604 windows was used to calculate PMF on the production run trajectories. The Weighted Histogram Analysis Method
605 (WHAM) was used, with default settings (50 bins and tolerance of $10^{-6} \text{ kJ mol}^{-1}$), using the gmh wham GROMACS
606 tool. The analysis of the simulation was carried out on the 150 ns production dynamics, during which configurations

607 were stored every 0.1 ns. The statistical uncertainty of the obtained PMF was estimated by bootstrapping analysis
608 [Hub 2010].

609 *Peptide stability in serum and in DMEM*

610 The peptides were dissolved in DMSO (5mg/mL). In eppendorf tubes, 1 mL of HEPES buffer (25 mM, pH = 7.6)
611 was temperature equilibrated at 37 °C before adding 250 µL of human serum and 20 µL of peptide solution; the
612 reaction was followed for 90 minutes. At fixed intervals, 100 µL of the solution were withdrawn and added to 200 µL
613 of absolute ethanol. These samples were kept on ice for 15 minutes, then centrifuged at 13,000 rpm for 5 minutes; the
614 supernatant solutions were analyzed by HPLC and HPLC-MS with 20-60% B gradient in 20 minutes to follow the
615 reaction. In parallel, samples containing peptide, buffer and ethanol only were analyzed. A degradation resistance test
616 was also conducted in DMEM (Dulbecco's Modified Eagle Medium). The experimental conditions are similar to
617 those described above; the reaction was followed for 72 hours. The enzymatic degradation resistance tests were
618 followed by HPLC using a 5-50% B gradient in 20 minutes.

619 *In vivo zebrafish rescue experiments*

620 One cell stage zebrafish embryos were injected with a mixture of 120 ng/µl of mRNA encoding either GFP-2A-Shp2-
621 D61G or GFP-2A-Shp2-wt (as a control), with or without OP, at 0.3 µM, 3 µM and 5 µM concentration. Embryos
622 were selected based on proper GFP expression and imaged at 11 hours post fertilization (hpf) in their lateral position
623 using the Leica M165 FC stereomicroscope. Images were analyzed using ImageJ [Schneider 2012], by measuring the
624 ratio of the major and minor axis from a minimum of 31 embryos. Statistical analysis was performed in GraphPad
625 Prism, using the analysis of variance (ANOVA) complemented by Tukey's honest significant difference test (Tukey's
626 HSD). To measure the survival of injected embryos, a minimum of 48 embryos per group were grown up to 4 days
627 post fertilization (dpf) and counted at 1 dpf and 4 dpf. Survival curves were plotted using GraphPad Prism, and the
628 differences between samples were determined using the Log-rank (Mantel-Cox) test.

629 References

- 630 Abraham, M.J. et al. (2015) GROMACS: High performance molecular simulations through multi-
631 level parallelism from laptops to supercomputers. *SoftwareX* 1-2, 19-25.
- 632 Anselmi, M., Calligari, P., Hub, J.S., Tartaglia, M., Bocchinfuso, G., Stella, L. (2020). Structural
633 Determinants of Phosphopeptide Binding to the N-Terminal Src Homology 2 Domain of
634 the SHP2 Phosphatase. *BioRxiv* 2020.03.27.012492; doi:
635 <https://doi.org/10.1101/2020.03.27.012492>
- 636 Araki, T., Mohi, M. G., Ismat, F. A., Bronson, R. T., Williams, I. R., Kutok, J. L., ... & Neel, B.
637 G. (2004). Mouse model of Noonan syndrome reveals cell type- and gene dosage-
638 dependent effects of Ptpn11 mutation. *Nature medicine*, 10(8), 849-857.
- 639 Bobone, S., Piazzon, A., Orioni, B., Pedersen, J. Z., Nan, Y. H., Hahm, K. S., ... & Stella, L.
640 (2011). The thin line between cell-penetrating and antimicrobial peptides: the case of Pep-
641 1 and Pep-1-K. *Journal of Peptide Science*, 17(5), 335-341.
- 642 Bocchinfuso, G., Stella, L., Martinelli, S., Flex, E., Carta, C., Pantaleoni, F., ... & Palleschi, A.
643 (2007). Structural and functional effects of disease-causing amino acid substitutions
644 affecting residues Ala72 and Glu76 of the protein tyrosine phosphatase SHP-2. *Proteins:
645 Structure, Function, and Bioinformatics*, 66(4), 963-974.
- 646 Bonetti, D., Troilo, F., Toto, A., Travaglini-Allocatelli, C., Brunori, M., & Gianni, S. (2018).
647 Mechanism of Folding and Binding of the N-Terminal SH2 Domain from SHP2. *The
648 Journal of Physical Chemistry B*, 122(49), 11108-11114.
- 649 Bradshaw, J. M., Grucza, R. A., Ladbury, J. E., & Waksman, G. (1998). Probing the “two-
650 pronged plug two-holed socket” model for the mechanism of binding of the Src SH2
651 domain to phosphotyrosyl peptides: a thermodynamic study. *Biochemistry*, 37(25), 9083-
652 9090.
- 653 Bradshaw, J. M., Mitaxov, V., & Waksman, G. (1999). Investigation of phosphotyrosine
654 recognition by the SH2 domain of the Src kinase. *Journal of molecular biology*, 293(4),
655 971-985.
- 656 Brooks, H., Lebleu, B., & Vivès, E. (2005). Tat peptide-mediated cellular delivery: back to
657 basics. *Advanced drug delivery reviews*, 57(4), 559-577.
- 658 Burke, J. T. (2006). Design and synthesis of phosphonodifluoromethyl phenylalanine (F2Pmp): a
659 useful phosphotyrosyl mimetic. *Current topics in medicinal chemistry*, 6(14), 1465-1471.
- 660 Bussi, G., Donadio, D., & Parrinello, M. (2007). Canonical sampling through velocity
661 rescaling. *The Journal of chemical physics*, 126(1), 014101.
- 662 Case, R. D., Piccione, E., Wolf, G., Benett, A. M., Lechleider, R. J., Neel, B. G., & Shoelson, S.
663 E. (1994). SH-PTP2/Syp SH2 domain binding specificity is defined by direct interactions
664 with platelet-derived growth factor beta-receptor, epidermal growth factor receptor, and
665 insulin receptor substrate-1-derived phosphopeptides. *Journal of Biological
666 Chemistry*, 269(14), 10467-10474.
- 667 Castanho, M. A., Santos, N. C., & Loura, L. M. (1997). Separating the turbidity spectra of
668 vesicles from the absorption spectra of membrane probes and other
669 chromophores. *European biophysics journal*, 26(3), 253-259.
- 670 Chen, Y. N. P., LaMarche, M. J., Chan, H. M., Fekkes, P., Garcia-Fortanet, J., Acker, M. G., ... &
671 Dobson, J. R. (2016). Allosteric inhibition of SHP2 phosphatase inhibits cancers driven by
672 receptor tyrosine kinases. *Nature*, 535(7610), 148.

- 673 Cunnick, J. M., Mei, L., Doupnik, C. A., & Wu, J. (2001). Phosphotyrosines 627 and 659 of Gab1
674 constitute a bisphosphoryl tyrosine-based activation motif (BTAM) conferring binding
675 and activation of SHP2. *Journal of Biological Chemistry*, 276(26), 24380-24387.
- 676 De Souza, D., Fabri, L. J., Nash, A., Hilton, D. J., Nicola, N. A., & Baca, M. (2002). SH2
677 domains from suppressor of cytokine signaling-3 and protein tyrosine phosphatase SHP-2
678 have similar binding specificities. *Biochemistry*, 41(29), 9229-9236.
- 679 Digilio, M. C., Conti, E., Sarkozy, A., Mingarelli, R., Dottorini, T., Marino, B., ... & Dallapiccola,
680 B. (2002). Grouping of multiple-lentiginos/LEOPARD and Noonan syndromes on the
681 PTPN11 gene. *The American Journal of Human Genetics*, 71(2), 389-394.
- 682 Esbjörner, E. K., Lincoln, P., & Nordén, B. (2007). Counterion-mediated membrane penetration:
683 cationic cell-penetrating peptides overcome Born energy barrier by ion-pairing with
684 phospholipids. *Biochimica et Biophysica Acta (BBA)-Biomembranes*, 1768(6), 1550-1558.
- 685 Elson, A. (2018). Stepping out of the shadows: Oncogenic and tumor-promoting protein tyrosine
686 phosphatases. *The international journal of biochemistry & cell biology*, 96, 135-147.
- 687 Fabrini, R., De Luca, A., Stella, L., Mei, G., Orioni, B., Ciccone, S., ... & Ricci, G. (2009).
688 Monomer– dimer equilibrium in glutathione transferases: a critical re-
689 examination. *Biochemistry*, 48(43), 10473-10482.
- 690 Fan, Z., Tian, Y., Chen, Z., Liu, L., Zhou, Q., He, J., ... & Xu, C. (2020). Blocking interaction
691 between SHP2 and PD-1 denotes a novel opportunity for developing PD-1
692 inhibitors. *EMBO Molecular Medicine*.
- 693 Fujioka, Y., Matozaki, T., Noguchi, T., Iwamatsu, A., Yamao, T., Takahashi, N., ... & Kasuga, M.
694 (1996). A novel membrane glycoprotein, SHPS-1, that binds the SH2-domain-containing
695 protein tyrosine phosphatase SHP-2 in response to mitogens and cell adhesion. *Molecular
696 and cellular biology*, 16(12), 6887-6899.
- 697 García-Gómez, R., Bustelo, X. R., & Crespo, P. (2018). Protein–protein interactions: Emerging
698 oncotargets in the RAS-ERK pathway. *Trends in cancer*, 4(9), 616-633.
- 699 Gracia, S. R., Gaus, K., & Sewald, N. (2009). Synthesis of chemically modified bioactive
700 peptides: recent advances, challenges and developments for medicinal chemistry. *Future
701 medicinal chemistry*, 1(7), 1289-1310.
- 702 Gu, H., Griffin, J. D., & Neel, B. G. (1997). Characterization of two SHP-2-associated binding
703 proteins and potential substrates in hematopoietic cells. *Journal of Biological
704 Chemistry*, 272(26), 16421-16430.
- 705 Hayashi, T., Senda, M., Suzuki, N., Nishikawa, H., Ben, C., Tang, C., ... & Hatakeyama, M.
706 (2017). Differential mechanisms for SHP2 binding and activation are exploited by
707 geographically distinct *Helicobacter pylori* CagA oncoproteins. *Cell reports*, 20(12),
708 2876-2890.
- 709 Henninot, A., Collins, J. C., & Nuss, J. M. (2018). The current state of peptide drug discovery:
710 back to the future?. *Journal of medicinal chemistry*, 61(4), 1382-1414.
- 711 Higashi, H., Tsutsumi, R., Muto, S., Sugiyama, T., Azuma, T., Asaka, M., & Hatakeyama, M.
712 (2002). SHP-2 tyrosine phosphatase as an intracellular target of *Helicobacter pylori* CagA
713 protein. *Science*, 295(5555), 683-686.
- 714 Hof, P., Pluskey, S., Dhe-Paganon, S., Eck, M. J., & Shoelson, S. E. (1998). Crystal structure of
715 the tyrosine phosphatase SHP-2. *Cell*, 92(4), 441-450.

- 716 Homeyer, N., Horn, A. H., Lanig, H., & Sticht, H. (2006). AMBER force-field parameters for
717 phosphorylated amino acids in different protonation states: phosphoserine,
718 phosphothreonine, phosphotyrosine, and phosphohistidine. *Journal of molecular*
719 *modeling*, 12(3), 281-289.
- 720 Huang, H., Li, L., Wu, C., Schibli, D., Colwill, K., Ma, S., ... & Pawson, T. (2008). Defining the
721 specificity space of the human SRC homology 2 domain. *Molecular & Cellular*
722 *Proteomics*, 7(4), 768-784.
- 723 Huang, X. (2003). Fluorescence polarization competition assay: the range of resolvable inhibitor
724 potency is limited by the affinity of the fluorescent ligand. *Journal of biomolecular*
725 *screening*, 8(1), 34-38
- 726 Hub, J. S., De Groot, B. L., & Van Der Spoel, D. (2010). g_wham - A Free Weighted Histogram
727 Analysis implementation Including Robust Error and Autocorrelation Estimates. *Journal*
728 *of chemical theory and computation*, 6(12), 3713-3720.
- 729 Hu, J., Liu, J., Ghirlando, R., Saltiel, A. R., & Hubbard, S. R. (2003). Structural basis for
730 recruitment of the adaptor protein APS to the activated insulin receptor. *Molecular*
731 *cell*, 12(6), 1379-1389.
- 732 Huyer, G., Li, Z. M., Adam, M., Huckle, W. R., & Ramachandran, C. (1995). Direct
733 determination of the sequence recognition requirements of the SH2 domains of SH-PTP2.
734 *Biochemistry*, 34(3), 1040-1049.
- 735 Imhof, D., Wavreille, A. S., May, A., Zacharias, M., Tridandapani, S., & Pei, D. (2006).
736 Sequence Specificity of SHP-1 and SHP-2 Src Homology 2 Domains CRITICAL ROLES
737 OF RESIDUES BEYOND THE pY+ 3 POSITION. *Journal of Biological*
738 *Chemistry*, 281(29), 20271-20282.
- 739 Jopling, C., van Geemen, D., & den Hertog, J. (2007). Shp2 knockdown and Noonan/LEOPARD
740 mutant Shp2-induced gastrulation defects. *PLoS genetics*, 3(12), e225.
- 741 Kaneko, T., Huang, H., Cao, X., Li, X., Li, C., Voss, C., ... & Li, S. S. (2012). Superbinder SH2
742 domains act as antagonists of cell signaling. *Science signaling*, 5(243), ra68-ra68.
- 743 Kay, L. E., Muhandiram, D. R., Wolf, G., Shoelson, S. E., & Forman-Kay, J. D. (1998).
744 Correlation between binding and dynamics at SH2 domain interfaces. *Nature structural*
745 *biology*, 5(2), 156.
- 746 Keilhack, H., David, F. S., McGregor, M., Cantley, L. C., & Neel, B. G. (2005). Diverse
747 Biochemical Properties of Shp2 Mutants. Implications for Disease Phenotypes. *Journal of*
748 *Biological Chemistry*, 280(35), 30984-30993.
- 749 Kertesz, A., Varadi, G., Toth, G. K., Fajka-Boja, R., Monostori, E., & Sarmay, G. (2006).
750 Optimization of the cellular import of functionally active SH2-domain-interacting
751 phosphopeptides. *Cellular and Molecular Life Sciences CMLS*, 63(22), 2682-2693.
- 752 Kratz, C. P., Niemeyer, C. M., Castleberry, R. P., Cetin, M., Bergsträsser, E., Emanuel, P. D., ...
753 & Sary, J. (2005). The mutational spectrum of PTPN11 in juvenile myelomonocytic
754 leukemia and Noonan syndrome/myeloproliferative disease. *Blood*, 106(6), 2183-2185.
- 755 Kulkarni, K., Sang, J., Ma, X., & Wilce, J. A. (2020). Comparison between clickable cyclic TAT
756 and penetratin for delivery of cyclic and bicyclic-peptide cargos. *Peptide Science*, e24163.
- 757 Kuriyan, J., & Cowburn, D. (1997). Modular peptide recognition domains in eukaryotic
758 signaling. *Annual review of biophysics and biomolecular structure*, 26(1), 259-288.

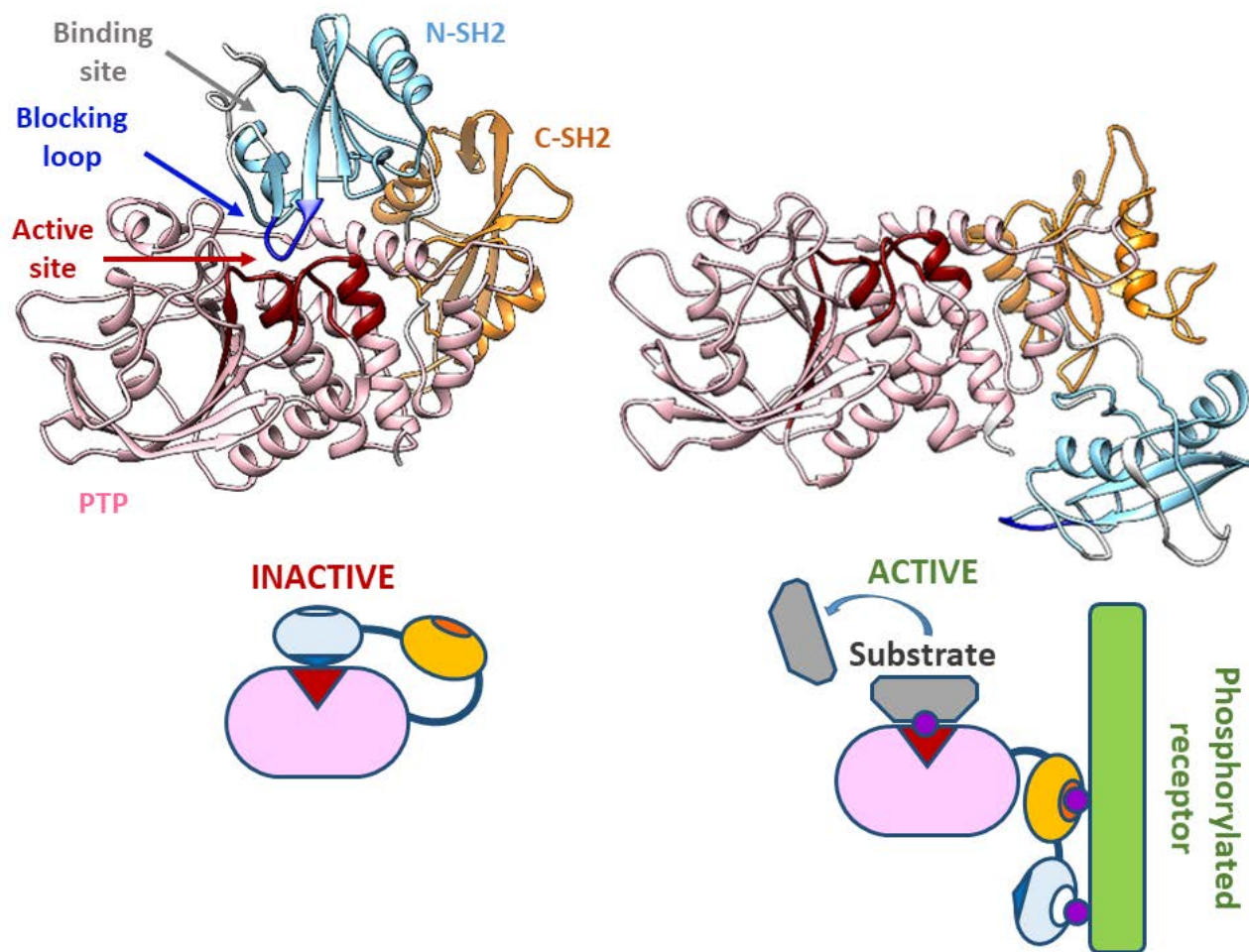
- 759 Ladbury, J. E., Lemmon, M. A., Zhou, M., Green, J., Botfield, M. C., & Schlessinger, J. (1995).
760 Measurement of the binding of tyrosyl phosphopeptides to SH2 domains: a
761 reappraisal. *Proceedings of the National Academy of Sciences*, 92(8), 3199-3203.
- 762 LaMarche, M. J., Acker, M. G., Argintaru, A., Bauer, D., Boisclair, J., Chan, H., ... & Doré, M.
763 (2020). Identification of TNO155, an Allosteric SHP2 Inhibitor for the Treatment of
764 Cancer. *Journal of Medicinal Chemistry*.
- 765 LaRochelle, J. R., Fodor, M., Vemulapalli, V., Mohseni, M., Wang, P., Stams, T., ... & Blacklow,
766 S. C. (2018). Structural reorganization of SHP2 by oncogenic mutations and implications
767 for oncoprotein resistance to allosteric inhibition. *Nature communications*, 9(1), 4508.
- 768 Lee, C. H., Kominos, D., Jacques, S., Margolis, B., Schlessinger, J., Shoelson, S. E., & Kuriyan,
769 J. (1994). Crystal structures of peptide complexes of the amino-terminal SH2 domain of
770 the Syp tyrosine phosphatase. *Structure*, 2(5), 423-438.
- 771 Liu, B. A., Jablonowski, K., Raina, M., Arcé, M., Pawson, T., & Nash, P. D. (2006). The human
772 and mouse complement of SH2 domain proteins—establishing the boundaries of
773 phosphotyrosine signaling. *Molecular cell*, 22(6), 851-868.
- 774 Machida, K., & Mayer, B. J. (2005). The SH2 domain: versatile signaling module and
775 pharmaceutical target. *Biochimica et Biophysica Acta (BBA)-Proteins and
776 Proteomics*, 1747(1), 1-25.
- 777 Marasco, M., Berteotti, A., Weyershaeuser, J., Thorasch, N., Sikorska, J., Krausze, J., ... &
778 Köhn, M. (2020). Molecular mechanism of SHP2 activation by PD-1 stimulation. *Science
779 advances*, 6(5), eaay4458.
- 780 Martinelli, S., Torreri, P., Tinti, M., Stella, L., Bocchinfuso, G., Flex, E., ... & Castagnoli, L.
781 (2008). Diverse driving forces underlie the invariant occurrence of the T42A, E139D,
782 I282V and T468M SHP2 amino acid substitutions causing Noonan and LEOPARD
783 syndromes. *Human molecular genetics*, 17(13), 2018-2029.
- 784 Martinelli, S., Nardoza, A. P., Delle Vigne, S., Sabetta, G., Torreri, P., Bocchinfuso, G., ... &
785 Cesareni, G. (2012). Counteracting effects operating on Src homology 2 domain-
786 containing protein-tyrosine phosphatase 2 (SHP2) function drive selection of the recurrent
787 Y62D and Y63C substitutions in Noonan syndrome. *Journal of Biological
788 Chemistry*, 287(32), 27066-27077.
- 789 Martinelli, S., Pannone, L., Lissewski, C., Brinkmann, J., Flex, E., Schanze, D., ... & Radio, F. C.
790 (2020). Pathogenic PTPN11 variants involving the poly-glutamine Gln255-Gln256-
791 Gln257 stretch highlight the relevance of helix B in SHP2's functional regulation. *Human
792 Mutation*.
- 793 Mullard, A. (2018). Phosphatases start shedding their stigma of undruggability. *Nature Reviews in
794 Drug Discovery*, 17(12):847-849.
- 795 Nasrolahi Shirazi, A., Tiwari, R. K., Oh, D., Banerjee, A., Yadav, A., & Parang, K. (2013).
796 Efficient delivery of cell impermeable phosphopeptides by a cyclic peptide amphiphile
797 containing tryptophan and arginine. *Molecular pharmaceutics*, 10(5), 2008-2020.
- 798 Noguchi, T., Matozaki, T., Horita, K., Fujioka, Y., & Kasuga, M. (1994). Role of SH-PTP2, a
799 protein-tyrosine phosphatase with Src homology 2 domains, in insulin-stimulated Ras
800 activation. *Molecular and cellular biology*, 14(10), 6674-6682.
- 801 Okazaki, T., Chikuma, S., Iwai, Y., Fagarasan, S., & Honjo, T. (2013). A rheostat for immune
802 responses: the unique properties of PD-1 and their advantages for clinical
803 application. *Nature immunology*, 14(12), 1212.

- 804 Pace, C. N., Vajdos, F., Fee, L., Grimsley, G., & Gray, T. (1995). How to measure and predict the
805 molar absorption coefficient of a protein. *Protein science*, 4(11), 2411-2423.
- 806 Park, S. C., Kim, M. H., Hossain, M. A., Shin, S. Y., Kim, Y., Stella, L., ... & Hahm, K. S.
807 (2008). Amphipathic α -helical peptide, HP (2–20), and its analogues derived from
808 *Helicobacter pylori*: pore formation mechanism in various lipid compositions. *Biochimica*
809 *et Biophysica Acta (BBA)-Biomembranes*, 1778(1), 229-241.
- 810 Pawson, T. (1995). Protein modules and signalling networks. *Nature*, 373(6515), 573-580.
- 811 Prahallad, A., Heynen, G. J., Germano, G., Willems, S. M., Evers, B., Vecchione, L., ... &
812 Bardelli, A. (2015). *PTPN11* is a central node in intrinsic and acquired resistance to
813 targeted cancer drugs. *Cell reports*, 12(12), 1978-1985.
- 814 Roberts, A. E., Allanson, J. E., Tartaglia, M., & Gelb, B. D. (2013). Noonan syndrome. *The*
815 *Lancet*, 381(9863), 333-342.
- 816 Roth, L., Wakim, J., Wasserman, E., Shalev, M., Arman, E., Stein, M., ... & Elson, A. (2019).
817 Phosphorylation of the phosphatase PTPROT at Tyr399 is a molecular switch that controls
818 osteoclast activity and bone mass in vivo. *Sci. Signal.*, 12(563), eaau0240.
- 819 Rönstrand, L., Arvidsson, A. K., Kallin, A., Rorsman, C., Hellman, U., Engström, U., ... &
820 Heldin, C. H. (1999). SHP-2 binds to Tyr763 and Tyr1009 in the PDGF β -receptor and
821 mediates PDGF-induced activation of the Ras/MAP kinase pathway and
822 chemotaxis. *Oncogene*, 18(25), 3696-3702.
- 823 Saxton, T. M., Henkemeyer, M., Gasca, S., Shen, R., Rossi, D. J., Shalaby, F., ... & Pawson, T.
824 (1997). Abnormal mesoderm patterning in mouse embryos mutant for the SH2 tyrosine
825 phosphatase Shp-2. *The EMBO journal*, 16(9), 2352-2364.
- 826 Sha, F., Gencer, E. B., Georgeon, S., Koide, A., Yasui, N., Koide, S., & Hantschel, O. (2013).
827 Dissection of the BCR-ABL signaling network using highly specific monoclonal inhibitors
828 to the SHP2 SH2 domains. *Proceedings of the National Academy of Sciences*, 110(37),
829 14924-14929.
- 830 Shi, Z. Q., Lu, W., & Feng, G. S. (1998). The Shp-2 tyrosine phosphatase has opposite effects in
831 mediating the activation of extracellular signal-regulated and c-Jun NH2-terminal
832 mitogen-activated protein kinases. *Journal of Biological Chemistry*, 273(9), 4904-4908.
- 833 Schneider, C. A., Rasband, W. S., & Eliceiri, K. W. (2012). NIH Image to ImageJ: 25 years of
834 image analysis. *Nature methods*, 9(7), 671-675.
- 835 Sugimoto, S., Lechleider, R. J., Shoelson, S. E., Neel, B. G., & Walsh, C. T. (1993). Expression,
836 purification, and characterization of SH2-containing protein tyrosine phosphatase, SH-
837 PTP2. *Journal of Biological Chemistry*, 268(30), 22771-22776.
- 838 Sugimoto, S., Wandless, T. J., Shoelson, S. E., Neel, B. G., & Walsh, C. T. (1994). Activation of
839 the SH2-containing protein tyrosine phosphatase, SH-PTP2, by phosphotyrosine-
840 containing peptides derived from insulin receptor substrate-1. *Journal of Biological*
841 *Chemistry*, 269(18), 13614-13622.
- 842 Tajan, M., de Rocca Serra, A., Valet, P., Edouard, T., & Yart, A. (2015). SHP2 sails from
843 physiology to pathology. *European journal of medical genetics*, 58(10), 509-525.
- 844 Takada, T., Matozaki, T., Takeda, H., Fukunaga, K., Noguchi, T., Fujioka, Y., ... & Kasuga, M.
845 (1998). Roles of the complex formation of SHPS-1 with SHP-2 in insulin-stimulated
846 mitogen-activated protein kinase activation. *Journal of Biological Chemistry*, 273(15),
847 9234-9242.

- 848 Tang, K., Jia, Y. N., Yu, B., & Liu, H. M. (2020). Medicinal Chemistry Strategies for the
849 Development of Protein Tyrosine Phosphatase SHP2 Inhibitors and PROTACs
850 Degraders. *European Journal of Medicinal Chemistry*, 112657.
- 851 Tartaglia, M., Mehler, E. L., Goldberg, R., Zampino, G., Brunner, H. G., Kremer, H., ... &
852 Kalidas, K. (2001). Mutations in PTPN11, encoding the protein tyrosine phosphatase
853 SHP-2, cause Noonan syndrome. *Nature genetics*, 29(4), 465.
- 854 Tartaglia, M., Niemeyer, C. M., Fragale, A., Song, X., Buechner, J., Jung, A., ... & Gelb, B. D.
855 (2003). Somatic mutations in PTPN11 in juvenile myelomonocytic leukemia,
856 myelodysplastic syndromes and acute myeloid leukemia. *Nature genetics*, 34(2), 148.
- 857 Tartaglia, M., Martinelli, S., Cazzaniga, G., Cordeddu, V., Iavarone, I., Spinelli, M., ... & Masera,
858 G. (2004). Genetic evidence for lineage-related and differentiation stage-related
859 contribution of somatic PTPN11 mutations to leukemogenesis in childhood acute
860 leukemia. *Blood*, 104(2), 307-313.
- 861 Tartaglia, M., Martinelli, S., Stella, L., Bocchinfuso, G., Flex, E., Cordeddu, V., ... & Sorcini, M.
862 (2006). Diversity and functional consequences of germline and somatic PTPN11
863 mutations in human disease. *The American Journal of Human Genetics*, 78(2), 279-290.
- 864 Tartaglia, M., & Gelb, B. D. (2010). Disorders of dysregulated signal traffic through the RAS-
865 MAPK pathway: phenotypic spectrum and molecular mechanisms. *Annals of the New
866 York Academy of Sciences*, 1214, 99.
- 867 Tinti, M., Kiemer, L., Costa, S., Miller, M. L., Sacco, F., Olsen, J. V., ... & Blom, N. (2013). The
868 SH2 domain interaction landscape. *Cell reports*, 3(4), 1293-1305.
- 869 Tóth, G. K., Bökönyi, G., Kéri, G., Pecht, I., Medgyesi, D., ... & Sármay, G. (2001). Co-
870 clustering of Fcγ and B cell receptors induces dephosphorylation of the Grb2-associated
871 binder 1 docking protein. *European journal of biochemistry*, 268(14), 3898-3906.
- 872 Tsutsumi, R., Ran, H., & Neel, B. G. (2018). Off-target inhibition by active site-targeting SHP 2
873 inhibitors. *FEBS open bio*, 8(9), 1405-1411.
- 874 Wagner, M. J., Stacey, M. M., Liu, B. A., & Pawson, T. (2013). Molecular mechanisms of SH2-
875 and PTB-domain-containing proteins in receptor tyrosine kinase signaling. *Cold Spring
876 Harbor perspectives in biology*, 5(12), a008987.
- 877 Waksman, G., Kumaran, S., & Lubman, O. (2004). SH2 domains: role, structure and implications
878 for molecular medicine. *Expert reviews in molecular medicine*, 6(3), 1-18.
- 879 Wang, M., Lu, J., Wang, M., Yang, C. Y., & Wang, S. (2020). Discovery of SHP2-D26 as a First,
880 Potent, and Effective PROTAC Degradator of SHP2 Protein. *Journal of Medicinal
881 Chemistry*, 63(14), 7510-7528.
- 882 Xu, D., Liu, X., Yu, W. M., Meyerson, H. J., Guo, C., Gerson, S. L., & Qu, C. K. (2011). Non-
883 lineage/stage-restricted effects of a gain-of-function mutation in tyrosine phosphatase
884 Ptpn11 (Shp2) on malignant transformation of hematopoietic cells. *Journal of
885 Experimental Medicine*, 208(10), 1977-1988.
- 886 Yu, Z. H., Zhang, R. Y., Walls, C. D., Chen, L., Zhang, S., Wu, L., ... & Zhang, Z. Y. (2014).
887 Molecular basis of gain-of-function LEOPARD syndrome-associated SHP2
888 mutations. *Biochemistry*, 53(25), 4136-4151.
- 889 Zeng, L. F., Zhang, R. Y., Yu, Z. H., Li, S., Wu, L., Gunawan, A. M., ... & Kapur, R. (2014).
890 Therapeutic potential of targeting the oncogenic SHP2 phosphatase. *Journal of medicinal
891 chemistry*, 57(15), 6594-6609.

892 Zhang, S. Q., Tsiaras, W. G., Araki, T., Wen, G., Minichiello, L., Klein, R., & Neel, B. G. (2002).
893 Receptor-specific regulation of phosphatidylinositol 3'-kinase activation by the protein
894 tyrosine phosphatase Shp2. *Molecular and cellular biology*, 22(12), 4062-4072.
895

896 **Acknowledgements:** the authors gratefully acknowledge the Protein Array and Analysis Core at
897 the MD Anderson Cancer Center for performing the SH2 array experiments. This work
898 was supported by AIRC Foundation for Cancer Research in Italy (grants IG19171, to L.S.
899 and IG21614, to M.T.), Italian Ministry of Education, University and Research (MIUR,
900 grant PRIN 20157WW5EH_007, to L.S.), Italian Ministry of Health (Ricerca Corrente
901 2019 and 2020, to M.T.), European Program on Rare Diseases (NSEuroNet, to M.T. and
902 J.d.H.), Partnership for Advanced Computing in Europe (PRACE, grants 2019204928 and
903 2017174118, to G. B.), which awarded computational resources at CINECA (Italy), and
904 CINECA (grant HP10BL5G4C, to G. B.). L.P. is a recipient of an AIRC research
905 fellowship. S. B., V. C., A. Q., G. T, G.C., A.B. and L.S. performed the binding studies
906 and participated to the protein purification; L.P., E.F., M.V., G.C., V.T., M.S. and S.M.
907 contributed the DNA constructs, protein production and purification, and the phosphatase
908 assays; B.B., C.D.F., T.G., C.P. and F.F. performed peptide synthesis and purification and
909 the experiments on peptide degradation; M. S., A. L., G. F., J. H. and J. d. H. contributed
910 the zebrafish experiments. P.C., V. S., L.S. and G. B. contributed the *in silico*
911 investigations; S.M., G.B., M.T. and L.S. conceived the study; L.S. coordinated the
912 research and wrote the manuscript. All the authors revised the article and contributed to its
913 writing. L.S., B.B., G.B., S.M. and M.T. are the inventors of a patent application, filed by
914 the University of Rome Tor Vergata and the Ospedale Pediatrico Bambino Gesù,
915 regarding the molecules described in the present article.
916
917



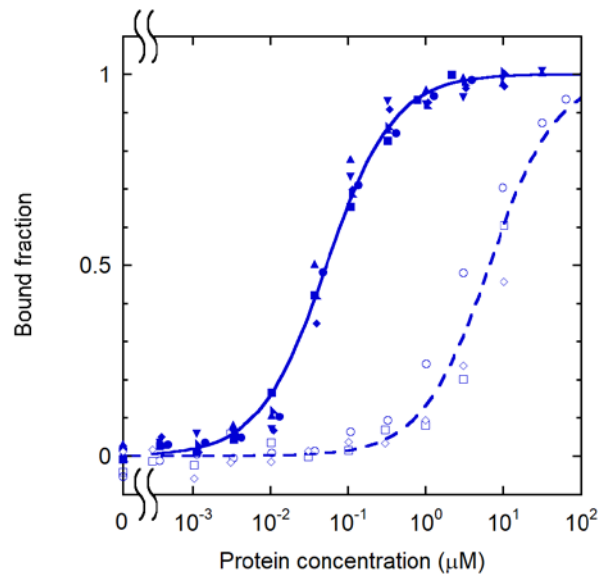
918

919 **Figure 1: SHP2 structure and scheme of the activation process.**

920 **Top:** crystallographic structures for the closed, auto-inhibited and the open, active states of SHP2
921 (left and right, respectively). The N-SH2, C-SH2 and PTP domain are colored in light blue,
922 orange and pink, respectively. The N-SH2 blocking loop (DE loop) is colored in blue, while the
923 PTP active site is highlighted in dark red. The EF and BG N-SH2 loops, controlling access to the
924 binding site for phosphorylated sequences of binding partners, are represented in white. PDB
925 codes of the two structures are 2SHP and 6CRF. Segments missing in the experimental structures
926 were modeled as previously described [Bocchinfuso 2007].

927 **Bottom:** schematic model of the allosteric regulation mechanism.

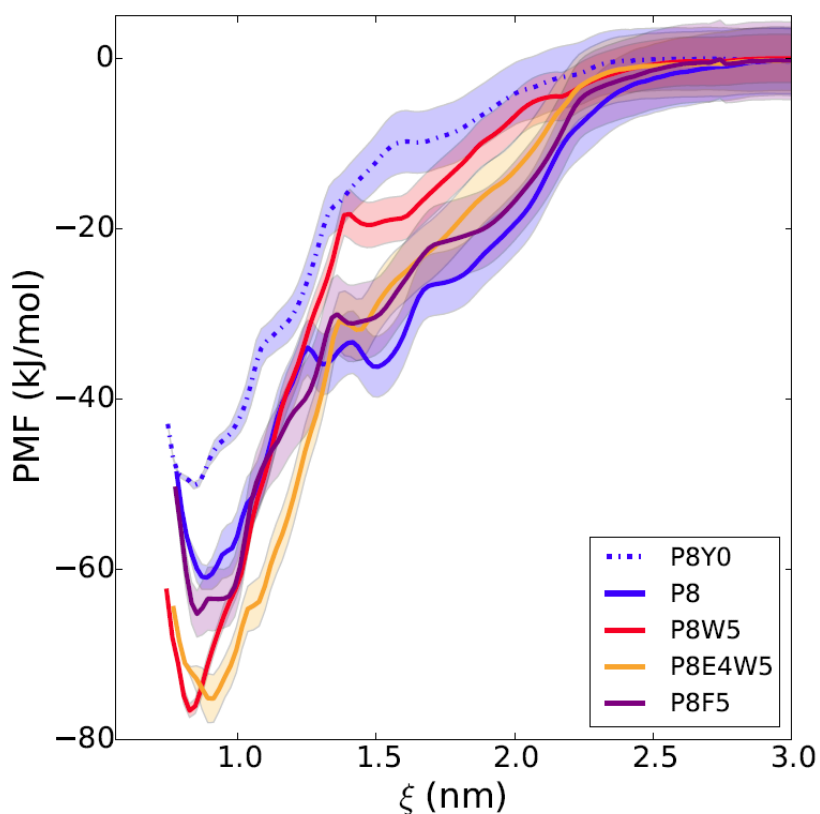
928



929

930 **Figure 2: Binding curves for the phosphorylated and unphosphorylated IRS-1 pY1172**
931 **peptides.**

932 [CF-P9]=1.0 nM (full symbols and solid line), [CF-P9Y0]=10 nM (empty symbols and dashed
933 line); Replicate experiments are reported with different symbols and were fit collectively.
934
935

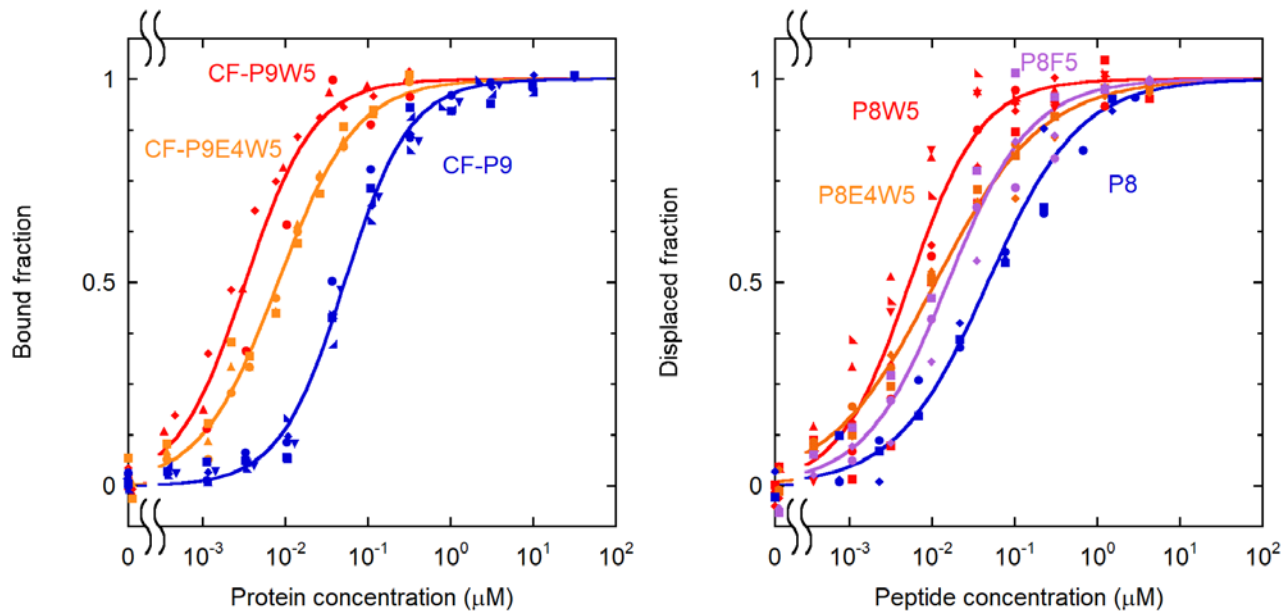


936

937 **Figure 3: in silico free energy calculations for different modified sequences**

938 The free energy profile is reported as a function of the distance between the centers of mass of the
939 N-SH2 domain and of the phosphopeptide. The simulations predict a loss in affinity of P8 (blue
940 line) with dephosphorylation of the pY (dashed blue line), and a gain with substitution of the L in
941 position +5 with W (red line), but not with F (violet line). The additional substitution of D in +4
942 with E (orange) does not provide any further increase in affinity. Shaded areas correspond to
943 standard deviations in the PMF profile.

944
945



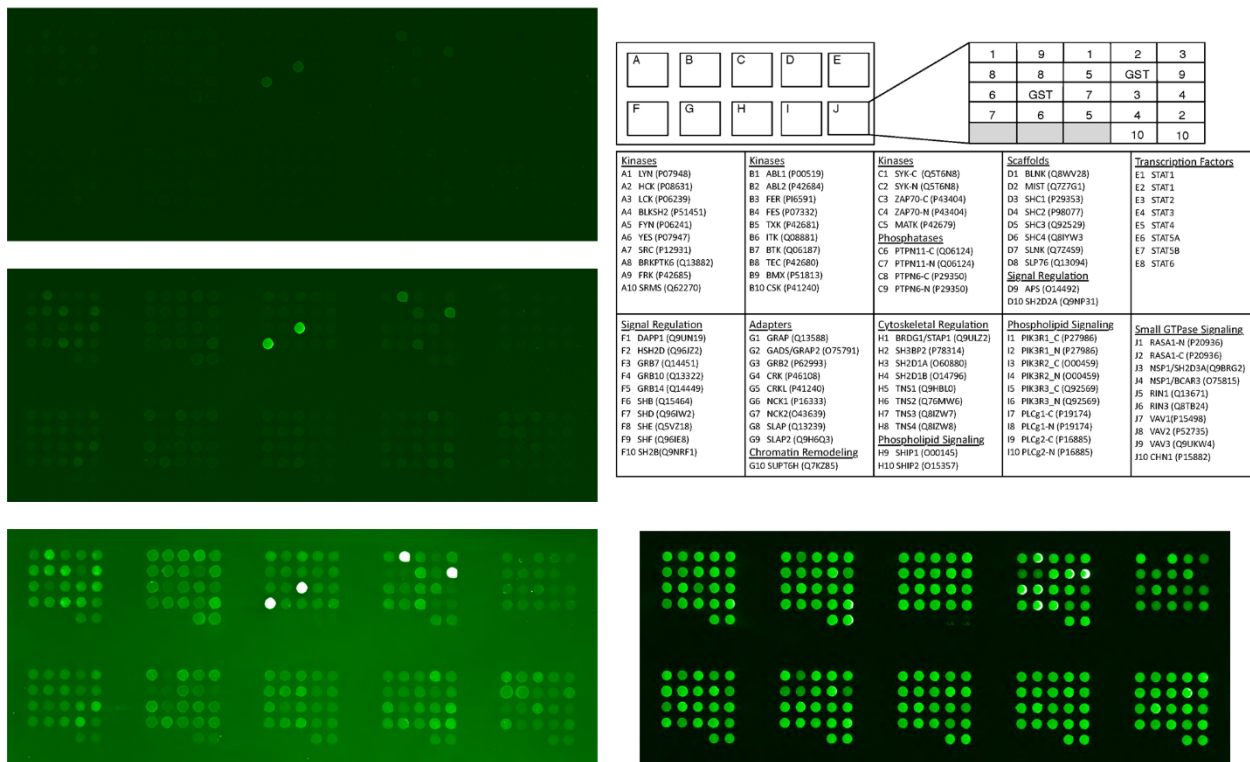
946

947 **Figure 4: effect of substitutions at position +5 on the binding affinity**

948 **Left:** direct binding experiments; [CF-P9W5]=0.10 nM, [CF-P9E4W5]=0.10 nM, [CF-P9]=1.0
949 nM. Data for CF-P9 are repeated here for comparison.

950 **Right:** displacement assay, [CF-P9W5]=0.10 nM, [N-SH2]=3.35 nM.

951



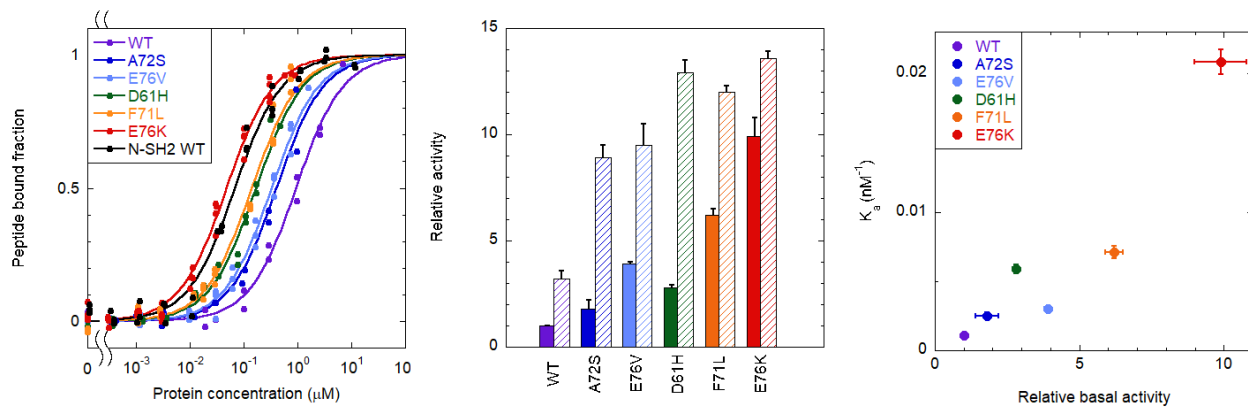
952

953 **Figure 5: binding selectivity of Cy3-P9W5 for an array of SH2 domains.**

954 **Left:** fluorescence of the bound peptide, at a concentration of 0.5 nM (top), 5.0 nM (center) and
 955 50 nM (bottom). Each SH2 domain was spotted in duplicate, and negative control spots (with
 956 GST only) are also present. The bright spots correspond to the N-SH2 domain of SHP2 and to the
 957 SH2 domain of the SH2 and PH domain-containing adapter protein APS (also called SHP2B2).
 958 The intensity of all other spots is comparable to that of the negative controls.

959 **Right:** position of each SH2 domain in the array (top), and control of the protein loading in each
 960 spot, performed with an anti-GST antibody (bottom).

961



962

963 **Figure 6: Binding of the CF-OP peptide to the whole SHP2 protein (WT and pathogenic**
964 **mutants)**

965 **Left:** fraction of CF-OP peptide bound to the WT protein and selected mutants, obtained from
966 fluorescence anisotropy experiments. The peptide bound fractions were obtained by following the
967 variation of the peptide fluorescence anisotropy during the titration with increasing amounts of
968 protein. [CF-OP]=1.0 nM.

969 **Center:** catalytic activity of the WT protein and selected mutants, under basal conditions (solid
970 bars) and after stimulation with 10 μM BTAM peptide (dashed bars). N=3

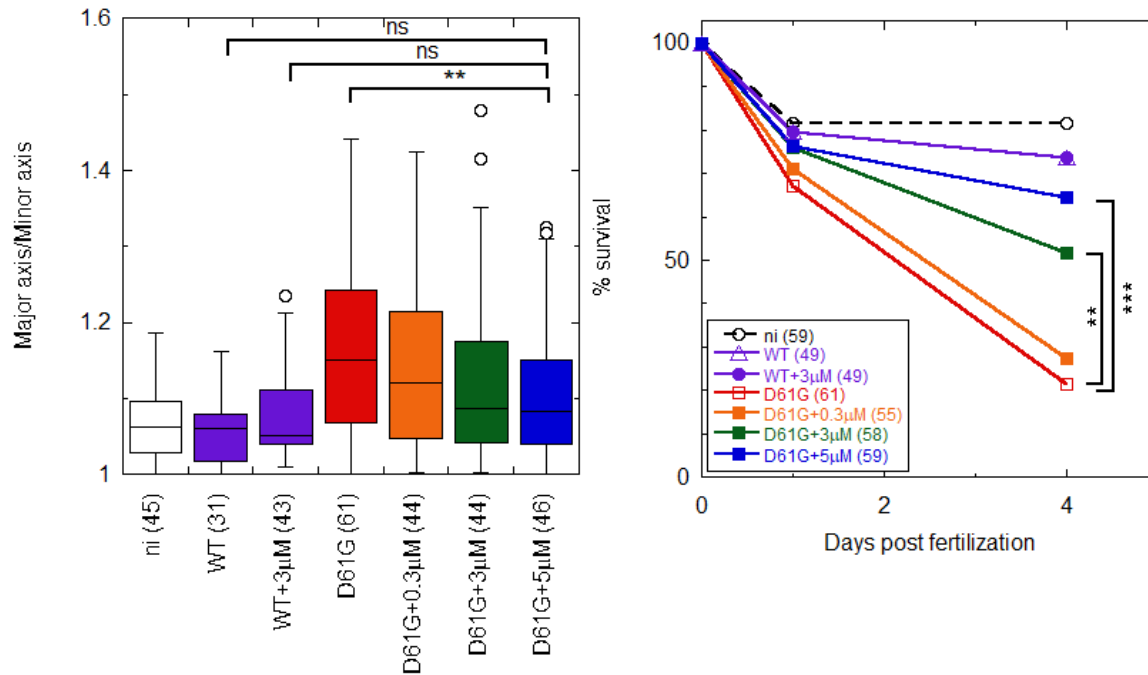
971 **Right:** correlation between basal activity and affinity (association constant).

972 Error bars represent standard deviations.

973

974

975



976

977 **Figure 7: the OP partially rescues Shp2a-D61G-induced gastrulation defects and mortality**
 978 **in a dose dependent manner in zebrafish embryos.**

979 Embryos were injected at the one-cell stage with mRNA encoding GFP-2A-Shp2-D61G or GFP-
 980 Shp2-wt with or without peptide at 0.3 μ M, 3 μ M and 5 μ M concentration. Non-injected embryos
 981 (ni) were evaluated as a control.

982 **Left:** ovality of embryos at 11 hpf, as indicated by the ratio of the long and the short axis. Tukey's
 983 honest significant difference test was done to assess significance. In the box plot, the horizontal
 984 line indicates the median, box limits indicate the 25th and 75th percentiles (interquartile range),
 985 whiskers (error bars) extend to the maximum and minimum values, or to 1.5 times the
 986 interquartile range from the 25th and 75th percentiles, if some data points fall outside this range. In
 987 the latter case, outliers are indicated as single data points.

988 **Right:** embryo lethality. Surviving embryos were counted at 1 dpf and 4 dpf. Survival was plotted
 989 and Log-rank test was done to access differences between groups.

990 Non significant (ns) $p > 0.05$; * $p < 0.05$; ** $p < 0.01$; *** $p < 0.001$. The number of embryos that
 991 were analyzed are indicated in parentheses.
 992

993

Table 1. Peptide sequences investigated in this study

Abbreviation	Sequence	R _t (min)	[M+H] ⁺	Purity
P9	GLN-pY-IDLDL	21.2 (10-40%B in30')	1156.5	95%
P9Y0	GLN- Y-IDLDL	10.9 (20-50%B in30')	1076.6	99%
P8	LN-pY-IDLDL	24.3 (10-40%B in30')	1099.4	92%
P7	N-pY-IDLDL	16.9 (10-40%B in30')	986.3	92%
P8W5	LN-pY-IDLDW	12.5 (20-60%B in20')	1172.5	95%
P8F5	LN-pY-IDLDF	16.5 (10-95%B in30')	1133.5	93%
P8E4W5	LN-pY-IDLEW	12.4 (20-60%B in 20')	1186.5	98%
P9ND0W5 (or OP)	GLN-ND-IDLDW	15.7 (10-50%B in20')	1263.4	94%
CF-P9	CF-GLN-pY-IDLDL	14.9 (20-50%B in30')	1473.5	93%
CF-P9Y0	CF-GLN- Y-IDLDL	18.7 (20-50%B in30')	1392.6	99%
CF-P9W5	CF-GLN-pY-IDLDW	14.0 (20-60%B in20')	1545.5	96%
Cy3-P9W5	Cy3-GLN-pY-IDLDW	19.6 (20-60%B in20')	1626.7	95%
CF-P9E4W5	CF-GLN-pY-IDLEW	13.9 (20-60%B in20')	1559.6	97%
CF-P9ND0W5 (or CF-OP)	CF-GLN-ND-IDLDW	16.1 (5-65%B in20')	1580.4	93%
P8W5-TAT	LN-pY-IDLDW-GRKKRRQRRR	16.1 (5-65%B in30')	2550.4	95%
CF-P9W5-TAT	CF-GLN-pY-IDLDW-GRKKRRQRRR	18.2 (5-65%B in30')	2924.6	90%

994

995

996

997

998

999

1000

1001

All peptides were amidated at the C-terminus. Unlabeled peptides were acetylated at the N-terminus. CF is 5,6 carboxyfluorescein, Cy3 is Cyanine 3 carboxylic acid and ND is the non-dephosphorylatable pY mimic phosphonodifluoromethyl phenylalanine (F₂Pmp). RP-HPLC retention times (R_t), molecular weights experimentally determined by ESI-MS spectrometry, and purities are reported. The RP-HPLC elution conditions used for each peptide are shown in parentheses. The optimized peptides are highlighted in grey.

1002 **Table 2. Dissociation constants obtained from the fluorescence anisotropy**
 1003 **binding experiments.**

Peptide	Domain/Protein	K_d (nM)
CF-P9	N-SH2	53 ± 2
CF-P9Y0	N-SH2	6600 ± 600
CF-P9W5	N-SH2	3.3 ± 0.2
CF-P9W5	C-SH2	4200 ± 300
Cy3-P9W5	N-SH2	23 ± 2
CF-P9E4W5	N-SH2	8.2 ± 0.7
CF-P9ND0W5 (CF-OP)	N-SH2	68 ± 5
CF-P9ND0W5 (CF-OP)	PTP	10000 ± 800
CF-P9ND0W5 (CF-OP)	SHP2 (WT)	930 ± 70
CF-P9ND0W5 (CF-OP)	SHP2 (A72S)	400 ± 40
CF-P9ND0W5 (CF-OP)	SHP2 (E76V)	330 ± 10
CF-P9ND0W5 (CF-OP)	SHP2 (D61H)	170 ± 10
CF-P9ND0W5 (CF-OP)	SHP2 (F71L)	140 ± 10
CF-P9ND0W5 (CF-OP)	SHP2 (E76K)	48 ± 2

1004
 1005
 1006

1007 **Table 3. Dissociation constants obtained from the displacement experiments**

Peptide	IC_{50} (nM)	K_i (nM)
P8	47 ± 4	22 ± 4
P8F5	16 ± 1	7 ± 2
P8W5	5.4 ± 0.3	1.5 ± 0.3
P8E4W5	11 ± 1	4 ± 2
P9ND0W5 (OP)	32 ± 5	14 ± 5

1008 All measurements were performed on the N-SH2 domain of SHP2. Experiments were performed
 1009 at [N-SH2]= 3.4 nM and [CF-P9W5]=0.5 nM (for P8 and P9ND0W5) or 0.1 nM (for the other
 1010 peptides)
 1011

Supplementary materials

For

Targeting Oncogenic Src Homology 2 Domain-Containing Phosphatase 2 (SHP2) by Inhibiting its Protein-Protein Interactions

S. Bobone, L. Pannone, B. Biondi, M. Solman, E. Flex, V. Canale, P. Calligari, C. De Faveri, T. Gandini, A. Quercioli, G. Torini, M. Venditti, A. Lauri, G. Fasano, J. Hoeksma, V. Santucci, G. Cattani, A. Bocedi, G. Carpentieri, V. Tirelli, M. Sanchez, C. Peggion, F. Formaggio, J. den Hertog, S. Martinelli, G. Bocchinfuso, M. Tartaglia, Lorenzo Stella.^{1,*}

Corresponding author: Lorenzo Stella

Email: stella@stc.uniroma2.it

Contents

Supplementary Materials and Methods

Figures S1 to S7

Table S1

Supplementary materials and methods

Analysis of binding curves

K_d values were obtained fitting the data with the following equation [Van de Weert 2011], which avoids the need for the commonly used (but often unjustified) approximation of the concentration of unbound protein with the total concentration:

$$\frac{r - r_0}{r_{max} - r_0} = \frac{[P]_T + [L]_T + K_d - \sqrt{([P]_T + [L]_T + K_d)^2 - 4[P]_T[L]_T}}{2[L]_T} \quad (1)$$

Here, $[P]_T$ and $[L]_T$ are the total protein and ligand concentrations, while r , r_0 and r_{max} are the anisotropy values at a given protein concentration, in the absence of protein and when the peptide is completely bound, respectively. When allowed by the experimental conditions (i.e. when $[L]_T \ll K_d$), this equation was simplified by assuming $[P]_T \cong [P]$ and obtaining:

$$\frac{r - r_0}{r_{max} - r_0} = \frac{[P]_t / K_d}{1 + [P]_t / K_d} \quad (2)$$

The affinity of unlabeled peptides was determined by competition experiments, in which a sample with fixed total protein and fluorescently labeled peptide concentrations ($[P]_T$ and $[L]_T$) was titrated with the unlabeled peptide, causing displacement of the fluorescent peptide and a decrease in anisotropy. From these data, the IC_{50} (i.e. the total concentration of unlabeled peptide that displaces half of the bound fluorescent analog) was determined, interpolating the displacement curve using a phenomenological Hill equation [Barlow 1989]:

$$\frac{r - r_0}{r_{fin} - r_0} = \frac{\left\{ [I]_T / IC_{50} \right\}^n}{1 + \left\{ [I]_T / IC_{50} \right\}^n} \quad (3)$$

where $[I]_T$ is the total concentration of the peptide causing the displacement, and r_{fin} is the anisotropy corresponding to total displacement, while in this case r_0 is the starting anisotropy, in the absence of displacing peptide.

Successively, the dissociation constant of the unlabeled peptide (K_i) was calculated from the known values of IC_{50} , K_d , $[P]_T$ and $[L]_T$, as described here below. Our treatment follows that of Nikolovska-Coleska [2004], through a slightly simplified route, and correcting some inaccuracies present in the equations of that article.

1055 In the system where protein (P), ligand (L) and a competitive inhibitor (I) are present, both L and I can form
 1056 complexes with P (PL and PI, respectively). The following dissociation constants can be defined for the two binding
 1057 equilibria:

$$1058 \quad K_d = \frac{[P][L]}{[PL]}; \quad K_i = \frac{[P][I]}{[PI]} \quad (4)$$

1059 and the following mass conservation laws apply:

$$1060 \quad [P]_T = [P] + [PI] + [PL]; \quad [L]_T = [L] + [PL]; \quad [I]_T = [I] + [PI] \quad (5)$$

1061 Let's define $[PL]_0$ as the complex concentration in the absence of inhibitor. Then, by definition, at the IC_{50}

$$1062 \quad [PL]_{50} = \frac{[PL]_0}{2} \quad (6)$$

1063 At the IC_{50} ,

$$1064 \quad \frac{[PL]_{50}}{[P]_T} = \frac{[PL]_{50}}{[P]_{50} + [PL]_{50} + [PI]_{50}} = \frac{1}{1 + \frac{[P]_{50}}{[PL]_{50}} + \frac{[PI]_{50}}{[PL]_{50}}} = \frac{1}{1 + \frac{[P]_{50}}{[PL]_{50}} \left(1 + \frac{[PI]_{50}}{[P]_{50}}\right)} \quad (7)$$

1065 and therefore

$$1066 \quad [PL]_{50} = \frac{[PL]_0}{2} = \frac{[P]_T}{1 + \frac{K_d}{[L]_{50}} \left(1 + \frac{[I]_{50}}{K_i}\right)} \quad (8)$$

1067 This equation can be inverted to calculate K_i

$$1068 \quad K_i = \frac{[I]_{50}}{\left(\frac{2[P]_T}{[PL]_0} - 1\right) \frac{[L]_{50}}{K_d} - 1} \quad (9)$$

1069 For $[L]_{50}$ we can write:

$$1070 \quad [L]_{50} = [L]_T - [PL]_{50} = [L]_T - \frac{[PL]_0}{2} \quad (10)$$

1071 Finally, for $[I]_{50}$ we can write:

$$1072 \quad [I]_{50} = IC_{50} - [PI]_{50} = IC_{50} - ([P]_T - [P]_{50} - [PL]_{50}) =$$

$$1073 \quad = IC_{50} - [P]_T + K_d \frac{[PL]_{50}}{[L]_{50}} + [PL]_{50} = IC_{50} - [P]_T + [PL]_{50} \left(1 + \frac{K_d}{[L]_{50}}\right) =$$

$$1074 \quad = IC_{50} - [P]_T + \frac{[PL]_0}{2} \left(1 + \frac{K_d}{[L]_T - \frac{[PL]_0}{2}}\right) \quad (11)$$

1075 Substituting the above equations in the expression for K_i , we get:

$$1076 \quad K_i = \frac{IC_{50} - [P]_T + \frac{[PL]_0}{2} \left(1 + \frac{K_d}{[L]_T - \frac{[PL]_0}{2}}\right)}{\left(\frac{2[P]_T}{[PL]_0} - 1\right) \frac{[L]_T - \frac{[PL]_0}{2}}{K_d} - 1} \quad (12)$$

1077 Finally, $[PL]_0$ can be substituted with the following expression, analogous to Eq. (1):

$$1078 \quad [PL]_0 = \frac{[P]_T + [L]_T + K_d - \sqrt{([P]_T + [L]_T + K_d)^2 - 4[P]_T[L]_T}}{2} \quad (13)$$

1079 In this way, K_i is expressed as a function of the known quantities IC_{50} , K_d , $[P]_T$ and $[L]_T$, without any approximation.

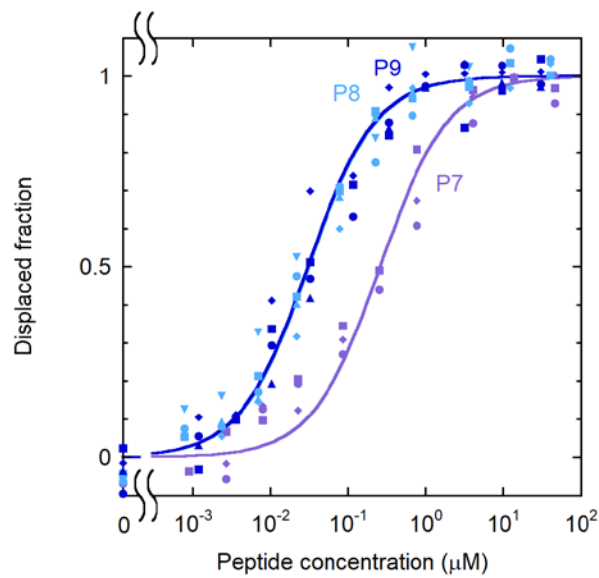
1080

1081 Barlow, R., & Blake, J. F. (1989). Hill coefficients and the logistic equation. Trends in
 1082 pharmacological sciences, 10(11), 440-441.

1083 Nikolovska-Coleska, Z., Wang, R., Fang, X., Pan, H., Tomita, Y., Li, P., ... & Wang, S. (2004).
 1084 Development and optimization of a binding assay for the XIAP BIR3 domain using
 1085 fluorescence polarization. Analytical biochemistry, 332(2), 261-273.

1086 Van de Weert, M., & Stella, L. (2011). Fluorescence quenching and ligand binding: A critical
 1087 discussion of a popular methodology. Journal of Molecular Structure, 998(1-3), 144-150.

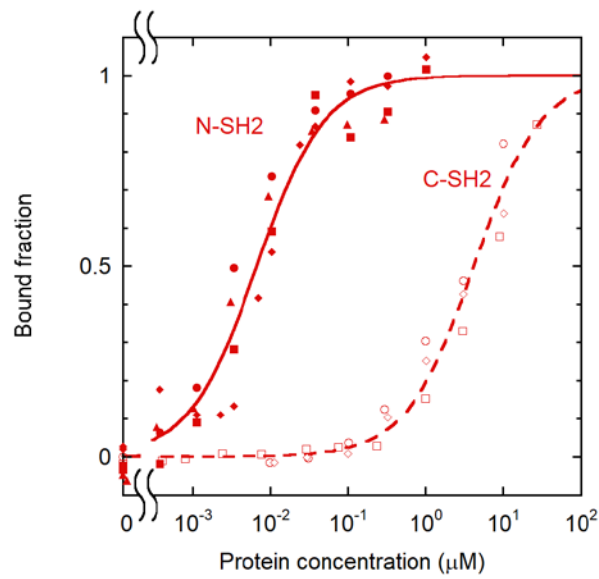
1088 **Supplementary figures**



1089

1090 **Figure S1: effect of sequence length on the binding affinity.**

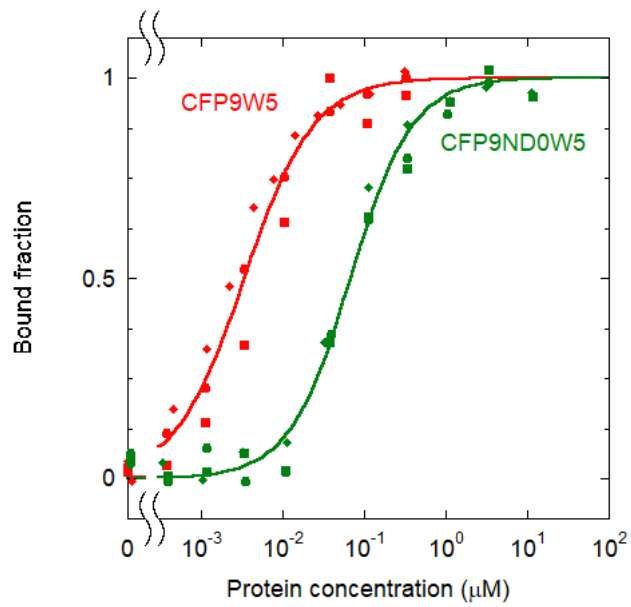
1091 Displacement experiments for analogs of different length. [CF-P9]=1.0 nM; [N-SH2]= 40 nM.



1092

1093 **Figure S2: binding selectivity of CF-P9W5 for the two SH2 domains of SHP2**

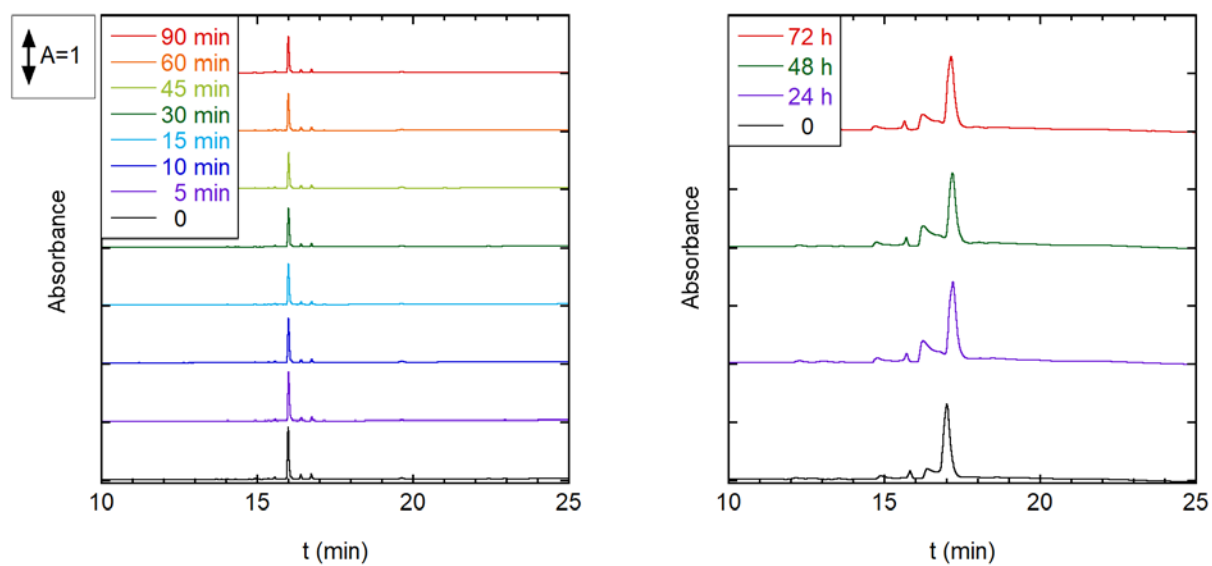
1094 Comparison of the association curves of CF-P9W5 to the N-SH2 and C-SH2 domains of SHP2.
1095 Experimental conditions for the N-SH2 binding experiments: see Fig. 5; for the C-SH2 binding
1096 experiments: [CF-P9W5]=1.0 nM.



1097

1098 **Figure S3: binding of the non-dephosphorylatable peptide CF-P9ND0W5 (or OP) to the N-**
1099 **SH2 domain.**

1100 For comparison, the curve for CF-P9W5 is also shown. [CF-P9ND0W5]=1.0 nM, [CF-
1101 P9W5]=0.10 nM.



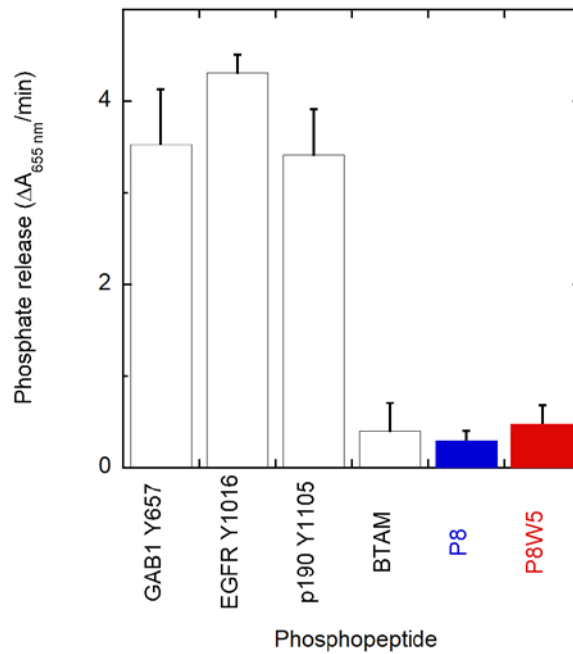
1102

1103 **Figure S4. OP resistance to proteolytic degradation in human serum and in DMEM**

1104 HPLC profiles of OP (CF-P9ND0W5), after incubation with human serum (left) or DMEM
1105 (right), for different times.

1106

1107



1108

1109 **Figure S5: dephosphorylation of P8W5 and other phosphopeptides by SHP2 Δ 104.**

1110 The following phosphopeptides were used for comparison, in addition to P8 and P8W5.

1111 GAB1 Y657 (DKQVEpYLDLDDL)

1112 p190A/RhoGAP Y1105 (EEENIpYSVPHD)

1113 EGFR Y1016 (VDADEpYLIPQQ)

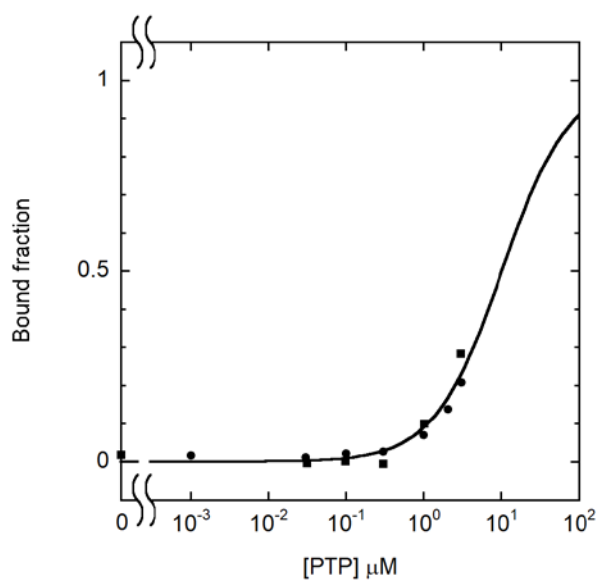
1114 BTAM, or bisphosphorylated SHSP-1 TAM1

1115 (GGGGDIT(pY)ADLNLPKGKKPAPQAAEPNNHTE(pY)ASIQTS, with 4 N-terminal G
1116 residues)

1117 A SHP2 construct lacking the N-SH2 domain (i.e. the first 104 residues, SHP2 Δ 104) was used at a
1118 95 nM concentration. Phosphopeptides were added at a 100 μ M concentration and the phosphate
1119 released was measured at different times. From the linear region of the phosphate versus time
1120 curve, the variation in absorbance at 655 nm in 1 min, due to phosphate release, was calculated
1121 and plotted.

1122

1123

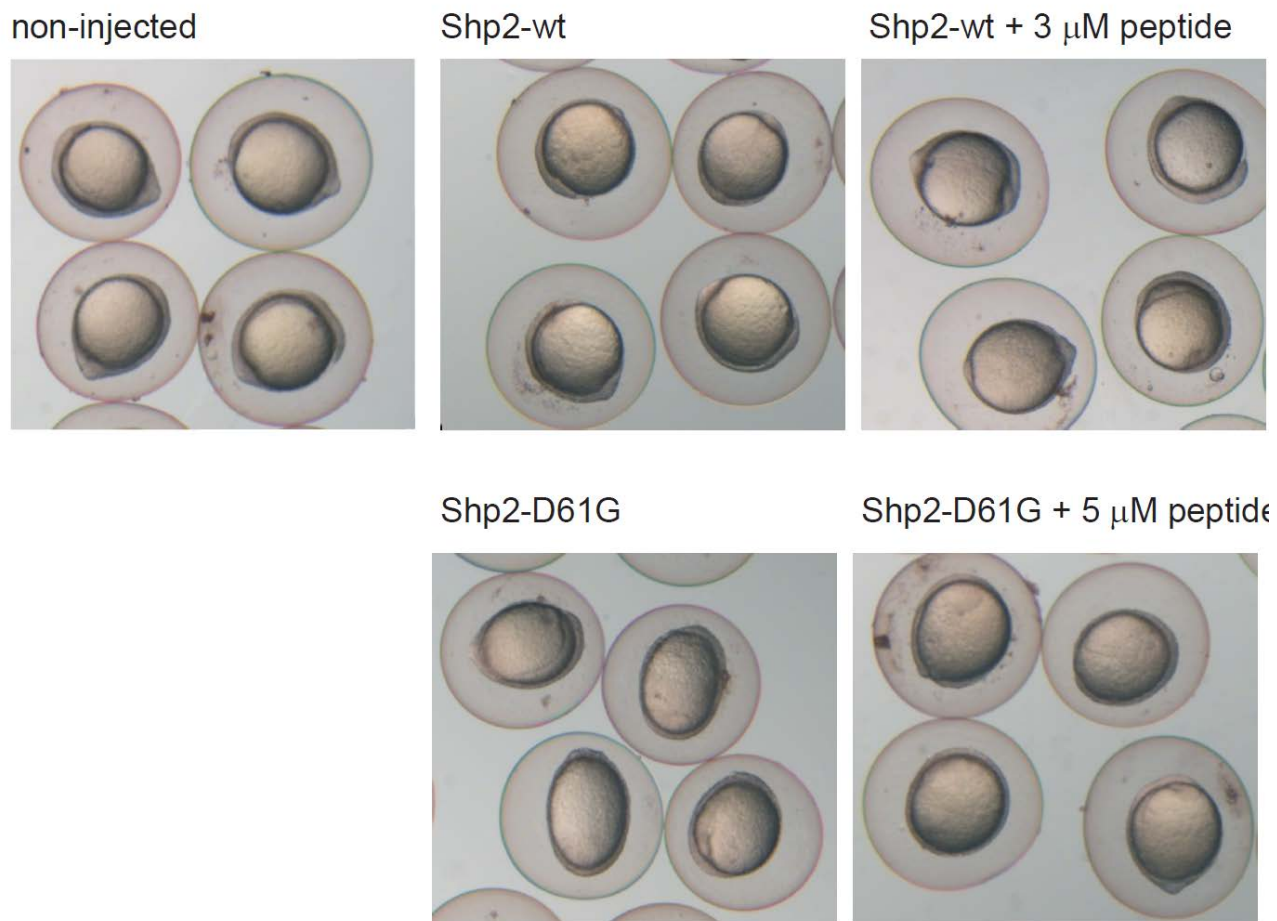


1124

1125 **Figure S6. CF-OP association to the PTP domain.**

1126 [CF-P9ND0W5]=1.0 nM

1127



1128

1129 **Figure S7. Representative images of zebrafish embryos at 11 hpf.**

1130 Embryos were injected at the one-cell stage with mRNA encoding GFP-2A-Shp2-D61G or GFP-
1131 Shp2-wt with or without peptide at 0.3 μ M, 3 μ M and 5 μ M concentration. Non-injected embryos
1132 (ni) were evaluated as a control.

1133

1134 **Supplementary tables**

1135 **Table S1. Literature values for IRS-1 pY1172/N-SH2 domain dissociation**
1136 **constant.**

Reference	Method	K _D
Case 1994	Radioactively labeled peptide	~1-10 μ M
Sugimoto 1994	SPR	14 \pm 8 nM
Keilhack 2005	ITC	51 nM

1137